

# Interlayer Exchange Coupling

M. D. Stiles

October 31, 2002

## 1 Introduction

Experiments in 1986 [1, 2, 3] demonstrated coupling between the magnetizations of two ferromagnetic layers separated by a non-magnetic spacer layer. Subsequent discoveries in these systems, including giant magnetoresistance [4, 5], led to an explosion in measurements and theories. The greatest interest has been in the simplest form of the coupling,

$$\frac{E}{A} = -J\hat{\mathbf{m}}_1 \cdot \hat{\mathbf{m}}_2, \quad (1)$$

called bilinear because the energy per area is linear in the directions of both magnetizations  $\hat{\mathbf{m}}_i$ . With this form of the interaction, positive values of the coupling constant  $J$  favor parallel alignment of the magnetizations and negative values favor antiparallel alignment. The discovery [6] that the sign of  $J$  and hence the preferred alignment of the magnetizations oscillates as the thickness of the spacer layer is varied accelerated the interest started by the discovery of giant magnetoresistance. The sign has been observed to change as many as sixty times [7] as the spacer layer thickness is varied between zero and eighty monolayers (see Fig. 3 below).

Chapter 2 of *Ultrathin Magnetic Structures II*, published in 1994, contains articles by Hathaway; Fert and Bruno; Pierce, Unguris, and Celotta; and Parkin reviewing aspects of interlayer exchange coupling [8]. These articles were written at a time of great evolution in our understanding. Shortly thereafter, a consensus developed on a theoretical model that unified many of the existing models. Simultaneously, high precision experiments were carried out enabling stringent tests of the theoretical models. In this chapter, I briefly summarize the situation that existed when these previous articles were written and then focus on the model that developed and measurements that were made shortly thereafter. For more details, see the earlier chapters [8] or other review articles [9, 10, 11, 12, 13, 14, 15].

By 1993, oscillatory interlayer exchange coupling had been measured in a large variety of systems. There had been measurements of a number of related effects including biquadratic coupling and quantum well states. Progress in growing high quality samples and measuring them accurately was evolving in parallel with the development of theoretical models. Systematic studies of multilayers grown by sputtering, typically with Co as the ferromagnet, had revealed oscillation periods in the range of 0.9 nm to 1.2 nm for V, Cu, Mo, Ru, Rh, Re, and Ir spacer layers [16, 17, 18, 19, 20] and longer periods of 1.5 nm for Os [21] and 1.8 nm for Cr [16]. Studies on lattice-matched systems grown by molecular-beam epitaxy (MBE) showed more complicated behaviors including much shorter periods. Examples include Co/Cu [22, 23, 24], Cr/Fe [25, 26, 27], Ag/Fe [28], Au/Fe [29].

There had been progress toward addressing two issues complicating the comparison between theory and experiment. One complication is the significant disorder that is present in real systems but absent in theoretical models. For one form of disorder, namely thickness fluctuations, averaging the interlayer exchange coupling over the growth front had been proposed [30] as a solution. Unfortunately, the growth front had not been measured and this correction had not been made quantitative. Progress on treating other types of disorder, like interdiffusion, was still to come. Another complication is that the thickness of the spacer layer can be both difficult to control and to measure with the desired accuracy. The use of wedge-shaped spacer layers [23, 31, 25], in which the thickness varies continuously, had been developed as a practical solution to this problem. Starting around the time the earlier reviews were written, there were a number of high precision measurements on wedge samples in which the sample quality was measured. These measurements have allowed stringent comparisons between theory and experiment.

Some samples had been shown to have a perpendicular alignment of the magnetizations [31, 32]. Phenomenologically, this alignment can be explained by the presence of a coupling between the magnetizations of the form

$$\frac{E}{A} = -J_2(\hat{\mathbf{m}}_1 \cdot \hat{\mathbf{m}}_2)^2, \quad (2)$$

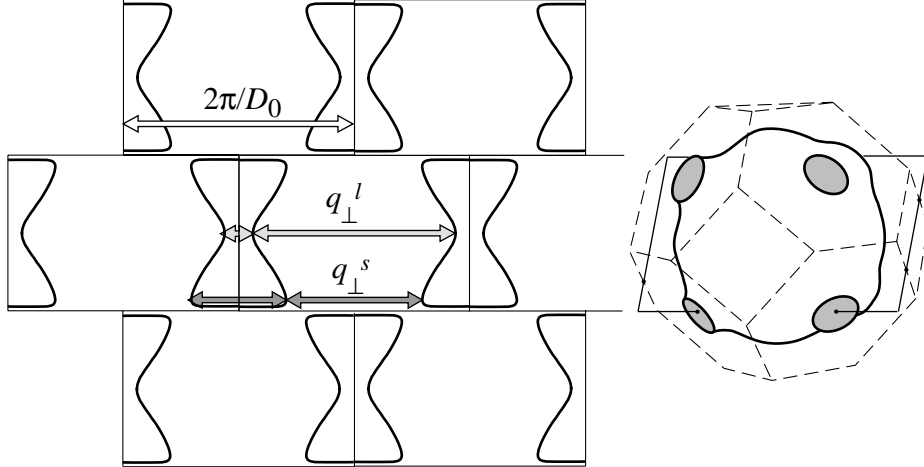


Figure 1: Critical spanning vectors for Cu in the 100 direction. The right panel shows a representation of the Cu Fermi surface and a rectangular slice (solid line) through it. The necks in the (111) directions are indicated in gray. The dashed lines indicate the bulk Brillouin zone. In the left panel, the rectangular slice from the right panel is repeated periodically using an extended zone scheme. There, the heavy curves show the Fermi surface of Cu in that slice. The white arrow gives a 1-dimensional reciprocal lattice vector in the interface direction. The gray arrows give the critical spanning vectors. An equivalent pair of vectors is shown for both the long ( $l$ ) and short ( $s$ ) period spanning vectors.

called biquadratic because it is quadratic in both of the magnetization directions. All measured values of  $J_2$  are negative, favoring perpendicular orientation of the two magnetizations. Biquadratic coupling has a separate origin from the bilinear coupling, in general coming from the presence of disorder [33]. In Section 4, I discuss this coupling and several of the models that have been proposed to explain it.

In addition to measurements of the coupling, there had been measurements of magnetic multilayers using photoemission and inverse photoemission [34, 35, 36, 37]. For these measurements, the sample consisted of a nonmagnetic layer on top of a magnetic layer. Strong peaks in the photoemission intensity were identified as arising from quantum well states. As the thickness of the top layer was varied, the quantum well states were observed to shift in energy. The periodicity in thickness at which these states crossed the Fermi level established a connection between the quantum well states and the interlayer exchange coupling.

By 1993, there were a number of theoretical models for interlayer exchange coupling. All gave the result that the Fermi surface of the spacer layer material [38] determined the coupling periods. In metals, the Fermi surface is a sharp cut-off in momentum space between filled states and unfilled states. In many contexts, the existence of this sharp cut-off gives rise to spatial oscillations. Well-known examples include Friedel oscillations of the charge density due to a localized perturbation and the Ruderman-Kittel-Kasuya-Yosida (RKKY) interaction between magnetic impurities [39]. The early models for oscillatory interlayer exchange coupling showed it to be an additional example.

The models showed that the critical spanning vectors of the Fermi surface of the spacer-layer material determine the oscillation periods. A spanning vector of the Fermi surface is a vector parallel to the interface normal that connects two points on the Fermi surface, one point having a positive component of velocity in the interface direction and the other a negative component. A *critical* spanning vector is a spanning vector that connects two sheets of the Fermi surface at a point where they are parallel to each other, see Fig. 1. For noble metal spacer layers, Bruno and Chappert [40] found the critical spanning vectors of Fermi surfaces that had been previously determined in de Haas-van Alphen measurements. The periods agree with the oscillations seen experimentally.

Since the spacer layer material is periodic, the Fermi surface is defined in a periodic Brillouin zone. After the discovery of oscillatory coupling, there was some doubt about whether the coupling was a Fermi surface effect because some early models ignored the lattice periodicity. The periods expected from free electron Fermi wave vectors are much smaller than the typically observed periods of 0.9 nm to 1.2 nm. Several groups [41, 42, 43] pointed out that *aliasing* would bring the periods into better agreement. Aliasing describes the result of periodically sampling an oscillating function. Here, the oscillating function is the oscillatory coupling and the periodic sampling occurs at the

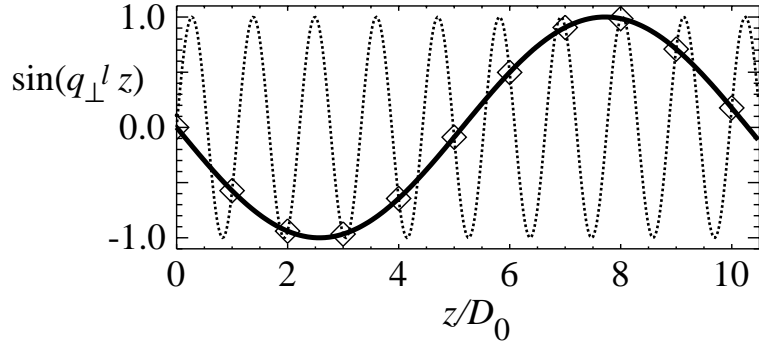


Figure 2: Aliasing. For the long period critical spanning vectors,  $q_{\perp}^l$ , illustrated in Fig. 1, the solid and dotted curves give the oscillations based on two equivalent choices for this vector. The squares give the values of both curves evaluated at the discrete layer thicknesses. At these points, the two curves are completely equivalent.

discrete layers thicknesses of  $nD_0$  where  $D_0$  is the individual layer thickness, and  $n$  is an integer. Figure 2 shows that the oscillation determined by the long period spanning vector  $q_{\perp}^l$  in Fig. 1 is equivalent to the oscillation determined by  $|q_{\perp}^l - g_0|$  where  $g_0 = 2\pi/D_0$  when both oscillations are evaluated at discrete layers  $z = nD_0$ . The wave vector  $g_0$  gives the appropriate length of the Brillouin zone in the interface direction. Some confusion can be avoided by always reducing the spatial frequency to its smallest equivalent magnitude.

If models are based on different descriptions of the electronic structure, the critical spanning vectors of the Fermi surface are different and the models predict different periods and different coupling strengths. When two models use the same electronic structure for the spacer layer and hence predict the same periods, they predict different coupling strengths if they use different descriptions for the electronic structure of the ferromagnetic layers.

In 1993, there was no consensus on the appropriate model for the interlayer exchange coupling because there was no consensus on the appropriate description of the electronic structure of transition metal multilayers. In the delocalized limit, all of the electrons are in band states. In the ferromagnet, the energy bands for majority and minority electrons are split by the exchange interaction. In the localized limit, the electrons are grouped into two sets, localized electrons that are spin polarized and delocalized electrons that couple to the localized magnetic electrons. These two limits emphasize different parts of the physics that are necessary for a correct description of ferromagnetism. One part is the hybridization between the electron states on different sites, and the other is the electron-electron interaction which is predominantly local.

The limit of completely localized magnetism was represented by models, related to the RKKY interaction between impurities, based on perturbative calculations of the  $s - d$  (or  $s - f$ ) Hamiltonian. In these models [30, 40, 44, 45], there are hybridized band states that interact with localized  $d$  states. The electron-electron interactions among the  $d$  states give rise to the magnetism. A more sophisticated approach to this limit is the Anderson model [46, 47], where the  $d$  levels become partially delocalized due to the hybridization with the  $s$  levels.

In the opposite limit of completely delocalized states, the simplest model is the free electron model [48, 49], which has the virtue of being analytically solvable. In this approximation, the bands in the ferromagnet are shifted in energy with respect to each other. The simplest case is to have the majority bands aligned with the bands of the spacer layer and the minority bands shifted infinitely high in energy. This limit is frequently called the infinite- $U$  limit. Edwards et al. [50] carried out closely related calculations for simple tight-binding models. Because the Fermi surfaces in tight-binding models are not spherical, their calculations make it clear that it is the critical spanning vectors, and not just the Fermi wave vectors that determine the oscillation periods. After the earlier reviews were written, a consensus developed that an accurate description of interlayer exchange coupling requires an accurate Fermi surface for the ferromagnet. This requirement necessitates a delocalized description (see Section 3).

The rest of this chapter focuses on developments since the previous volume of this series was written. Section 2 describes growth of the samples and some of the experimental techniques used to measure the coupling. Section 3 presents the model used to describe the interlayer coupling. Predictions of this model are compared to experiment. Disorder is discussed from an experimental point of view in Section 2 and from a theoretical point of view in Section 3. Disorder can introduce other types of coupling into these systems, in particular biquadratic coupling. Section 4 describes these other forms of coupling. Finally, Section 5 discusses calculations and measurements on

specific systems including Co/Cu(100), Au/Fe(100), and Cr/Fe in terms of this model.

## 2 Experiment

### 2.1 Sample growth

To make measurements that quantitatively test our understanding of interlayer exchange coupling, it is important to grow samples that are as close as possible to those assumed in theoretical treatments. These assumptions are usually quite restrictive. A typical calculation of interlayer exchange coupling assumes that the ferromagnet and the spacer layer are coherent, that is, they share a common lattice in the plane of the interface between them. Further, most (but not all) calculations assume that there are no defects either at the interface or in the bulk. Growing samples that approach this ideal is quite challenging. An alternative to eliminating defects is to quantify them. If the type and distribution of defects is well measured, then the burden is on the theorists to treat the imperfect system rather than the perfect one. However, it is also quite difficult to measure the defects in sufficient detail.

The first consideration in choosing an experimental system is to find a spacer layer that is close to lattice matched with a transition metal ferromagnet, Fe, Co, or Ni. When thin enough, a metal layer frequently assumes the in-plane lattice constant of the substrate on which it is deposited. This is coherent growth. As the thickness of the deposited layers increases, the strain energy associated with its modified lattice structure becomes too large and the film relaxes by introducing dislocations at the interface. To avoid dislocations, it is necessary to start with a pair of materials that have very similar lattice constants. Unfortunately, there are very few.

The most commonly studied systems are Fe/Cr and Co/Cu. Cr and Fe, which both take the body-centered cubic crystal structure, have less than one percent lattice mismatch, so can grow coherently to fairly large thicknesses. Since they have the same crystal structure they can be studied in several interface orientations, particularly (100), (110), and (211). Co naturally takes the hexagonal-close-packed (hcp) structure. However, when it grows on Cu, it frequently grows in the face-centered-cubic (fcc) structure of Cu (pseudomorphic growth) with a lattice mismatch of less than one percent, and so can also grow coherently to large thicknesses. Here also, a number of interface orientations have been investigated, particularly (100), (110), and (111). However, in the (111)-orientation the energy difference between fcc growth and hcp growth comes only from different stacking of hexagonal planes and hence is very small. Both types of growth tend to occur, leading to extended defects between different regions and very poor growth. For a review of growth in this system see [51].

Two other systems for which coherent growth can be achieved up to large thicknesses are Ag/Fe and Au/Fe. At first glance, these pairs are not only poorly lattice matched, but they do not have the same crystal structure. However, the (100) interface lattices of the noble metal and of the Fe differ by less than one percent, if the noble metal lattices are rotated by  $45^\circ$  with respect to that of Fe [29, 52]. If the starting substrates are sufficiently flat, very good growth can be achieved. However, the presence of steps leads to extended defects through the layer because the growth is not pseudomorphic and the layer thicknesses are quite different.

Other material pairs have been studied. An interesting pair is Fe/Cu. For thin enough layers, Fe grows in a face-centered-tetragonal structure (almost pseudomorphic) on Cu. Alternatively, Cu grows in a distorted body-centered-cubic (bcc) structure on Fe for thin enough layers. Thus, it is possible to study interlayer exchange coupling for bcc Cu [23, 28]. Transition metal spacer layers such as Fe/Pd [53], Fe/Nb [54], and Fe/Mo [55] have been grown by MBE. The same quality of growth has not been achieved in these systems as in the systems with much smaller lattice mismatch.

Even when the lattice mismatch is close to zero, the multilayers are still not perfect. The starting substrate is never perfectly flat and the growth is never perfectly layer by layer, so there are always variations in the thickness of the layers, typically called thickness fluctuations. If the growth front is measured, it is possible to account for the variations of the spacer layer thickness when comparing theory and experiment by averaging over the contributions from different thicknesses. However, when the interlayer exchange coupling has rapid oscillations, the measured coupling is significantly modified by the thickness fluctuations. Even for reasonably good growth, thickness fluctuations can completely obscure the experimental signature of short period oscillations in the coupling. For this reason, it is desirable to grow the sample in a layer-by-layer mode to keep the growth front as narrow as possible. Since layer-by-layer growth is determined by the competition between nucleation of islands and diffusion of deposited adatoms, it tends to require higher substrate temperatures during growth. Unfortunately, higher growth temperatures tend to promote interdiffusion at the interfaces. Such interdiffusion has been observed both for Cr growth on

Fe [56, 57, 58, 59] and Fe growth on Cu [60]. Interdiffusion, which gives rise to scattering centers, is more difficult to treat theoretically than thickness fluctuations. It also can be more difficult to measure.

In addition to the lattice matching between materials in the multilayer, the choice of substrate plays a large role in the quality of the growth. If substrates of one of the materials in the multilayer are available, they are frequently the best choice. Iron whiskers, which can be extremely flat [61], and copper single crystals are examples. However, these choices are not appropriate for transport measurements, like giant magnetoresistance, because the substrate provides a short circuit that prohibits any measurement of the transport properties of the multilayer. In this case, insulating substrates like MgO or semiconducting substrates like Si or GaAs can be used. For these substrates, great care is required to get really high quality growth. See [62] and [63] for descriptions of the complexity of growing a Fe/Au multilayer on a GaAs substrate.

As mentioned in the introduction, the difficulties in growing samples with particular spacer-layer thicknesses and in measuring those thicknesses are most easily addressed by growing wedge-shaped samples. To grow such samples, a shutter between the sample and the evaporator is moved to expose different parts of the sample to different total fluxes. After the wedge has been grown, Reflection High Energy Electron Diffraction (RHEED) (see Chapter 5 of Volume I of this series for details) can be used to determine the thickness of the sample at various positions along the wedge. RHEED is a commonly used technique for monitoring the quality and amount of growth. A high energy electron beam is reflected from the surface at glancing angles. The resulting diffraction pattern is sensitive to the details of the surface, in particular the presence of steps. If the growth is layer by layer, there are fewer steps when layers are close to complete and more when the layer is half filled. In this case, the intensity of different spots in the RHEED pattern oscillate with a period of one layer. In typical use, RHEED is used to monitor the thickness of a film during growth. However, for wedge samples, it is typically used after growth, when the RHEED beam is scanned along the wedge and the RHEED oscillations are monitored as a function of position to give the thickness at that position, see Fig. 3.

## 2.2 Measurement techniques

Interlayer exchange coupling is not measured directly. Rather, some magnetic property of a sample, like its hysteresis loop, is measured and the exchange coupling is inferred by comparing the measured property with a model. Some or all of the parameters of the model, including the interlayer layer coupling constant, are varied until the predictions of the model agree with the measurement. The reliability of the results depend on the accuracy of the model, in particular whether it includes all of the physics necessary to describe the experiment. In addition to the interlayer coupling, the models usually include the magnetic anisotropy of each of the layers. Typically, models assume coherent rotation, at least within each layer, so that the intralayer exchange interaction does not play a role. Magnetostatic effects are typically not included in the models. Hysteretic effects are usually ignored. That is, the “hysteresis loop” is calculated from a global energy minimum so there is no hysteresis in the model. At the same time, hysteresis that shows up in the measurement is averaged over to give a similar “loop” to compare to.

Measurements of interlayer exchange coupling fall into two broad classes. In the first class, the hysteresis loop (or some part) is measured. For example, Parkin et al. first observed oscillatory interlayer exchange coupling [6] using the giant magnetoresistance to determine the relative orientation of the magnetic layers. Here the resistance of the film in zero field was compared with the resistance in large field. If the coupling is ferromagnetic, there is no change, and if the coupling is antiferromagnetic the change can be substantial. The field required to saturate the resistance is used to estimate the strength of the antiferromagnetic coupling.

One technique commonly used to measure the hysteresis loop is the Magneto-Optic Kerr Effect (MOKE) (see Chapter 4 of Volume II of this series for details or [64]). MOKE can be used in an imaging mode by scanning the focused spot of a laser across the surface or by imaging a wide area of illumination. It is not particularly surface sensitive and has the advantage that it is sensitive to the magnetic state of both layers. Using the sensitivity to both layers, MOKE images [31] have directly identified perpendicular alignment of two layers.

Another imaging technique that has contributed significantly to understanding interlayer exchange coupling is Scanning Electron Microscopy with Polarization Analysis (SEMPA) (see Chapter 2 of Volume II of this series for details). Since this technique is based on measuring secondary electrons, it is generally not used with an applied field, limiting it to studies of the remnant state. On the other hand, it has greater spatial resolution than optical techniques like MOKE, and can be used on smaller wedges, requiring smaller areas of sample perfection. Since it can only measure the remnant state, SEMPA has not been used to measure coupling strengths, but it has been used to determine the sign of the coupling for enough oscillations of the coupling to allow high precision measurements of

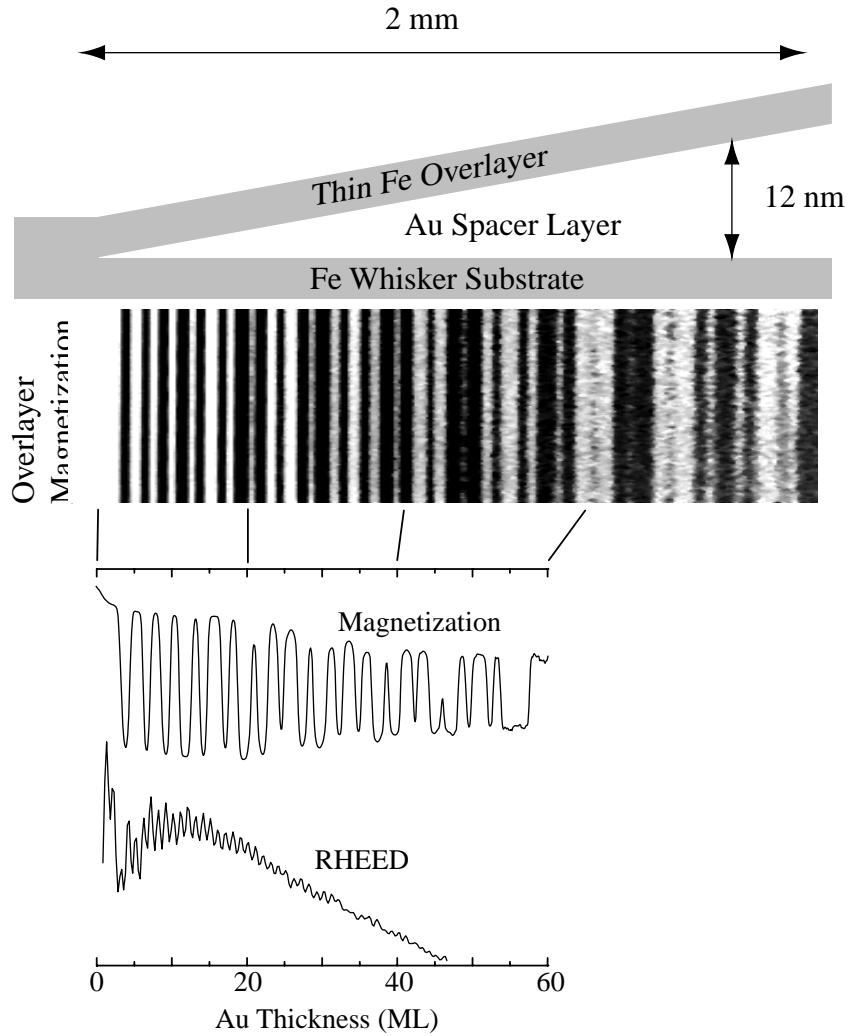


Figure 3: SEMPA image of coupling in Fe/Au/Fe with geometry and RHEED. A schematic view of the wedge-shaped sample is shown at the top of the figure. The approximate dimensions give an indication of the very small slope of the wedge. Immediately below is a SEMPA image of the magnetization of the Fe overlayer. White and black indicate parallel and antiparallel alignment to the substrate, and hence ferromagnetic and antiferromagnetic coupling. Below that is a line scan through the image and then a measurement of the RHEED intensity along the wedge. The oscillations are used to determine the thickness of the spacer layer along the wedge. Examination of the oscillations indicate that the slope of the wedge is not constant, but the wedge is slightly curved. The RHEED and the magnetization curves have been corrected for this curvature, but the image has not, hence the variation of the lines connecting the image with the line scan.

the periods.

The other class of measurements is based on determining the curvature of the energy with respect to small variations in the magnetization direction. Two such techniques are Ferromagnetic Resonance (FMR) and Brillouin Light Scattering (BLS) (see chapter 3 of Volume II of this series for details of both). In a multilayer structure, certain resonances, whether as a function of field at fixed frequency (FMR) or frequency at fixed field (BLS), depend on the strength of the interlayer coupling. The resonance positions can be used to determine the coupling.

### 3 Physical mechanism for bilinear coupling

In 1993, a model for interlayer exchange coupling [65, 66, 67] based on spin-dependent reflection at interfaces provided a framework to unify previous models for exchange coupling. This model is closely related to the model of Mathon et al. [68], formulated in terms of normalized spectral densities. Since the electron states in 3d transition metals are strongly hybridized, a delocalized description is necessary to accurately compute the interface reflection amplitudes. This fact led to a consensus that a delocalized description of the electronic structure of the 3d transition metals is more appropriate for models of interlayer exchange coupling. In this section, I present the model that led to this consensus.

First, the necessity of a delocalized description of transition metal ferromagnetism raises the question that frequently starts many discussions of interlayer exchange coupling: Is the coupling RKKY? The answer depends on what is meant by RKKY. If the most general sense is meant, that the oscillations of the coupling are due to the sharp cut-offs in momentum space due to the Fermi surface of the spacer layer, then the answer is yes. If the more restrictive sense is meant, that a perturbative treatment of an  $s - d$  Hamiltonian gives an adequate description of transition metal ferromagnetism, then the answer is no. The model I describe below is an RKKY model in the first, general sense, but not in the second, more restrictive sense.

From Eq. (1), the interlayer coupling constant is given by the difference in energy between the antiparallel alignment of the magnetizations and the parallel alignment

$$J = \frac{1}{2A}(E_{\text{anti}} - E_{\text{par}}). \quad (3)$$

Computing the interlayer exchange coupling is reduced to computing the energy difference between two configurations. Some calculations of interlayer exchange coupling evaluate these total energies directly using the local-spin-density approximation (LSDA) [69, 70] or various tight-binding models [71, 72]. Because the exchange coupling is much smaller than the total electronic energy for either alignment, it can be difficult to converge these calculations numerically.

Calculation of the energy differences in Eq. (3) can be significantly simplified by using the “force theorem.” First, let me stress the difficulty of carrying out self-consistent calculations of the total energies in (3) to sufficient accuracy to make the energy difference meaningful. The difficulty arises from treating the electron-electron interaction, even though it is only in mean field theory. The force theorem provides a way to avoid these self-consistent calculations. It states that the energy difference between two configurations is approximately given by the difference in the single particle energies in the two configurations. One simply develops approximations for the potential and then computes the sum of the single particle energies for each configuration. This approach ignores any explicit calculation of the electron-electron interactions. The force theorem states that if the approximations for the potential are good enough, the difference in energy of the single-particle-energy sums is very close to the difference in the fully self-consistent energies. Fortunately, it is fairly simple to develop good enough approximations for the potential because of the short range of the screening in metals. For thick enough layers, the potential in the middle of each layer can be treated as independent of the rest of the system and the potential near each interface as independent of the other interfaces. Thus, a good approximate potential for a multilayer can be constructed piece-wise from much smaller systems. Alternately, the potential can be found for the case of parallel alignment and then simply modified to give an approximate potential for antiparallel alignment.

Another feature of the force theorem is its pedagogical value. In the rest of the section, I develop a model for interlayer exchange coupling based on differences in the single particle energies. The force theorem allows me to ignore (to a good approximation) the complications of the electron-electron interactions.

The calculation is further simplified when spin-orbit coupling is neglected. Then, since the magnetizations are collinear for both the antiparallel and the parallel alignments, the majority and minority spins do not interact, and

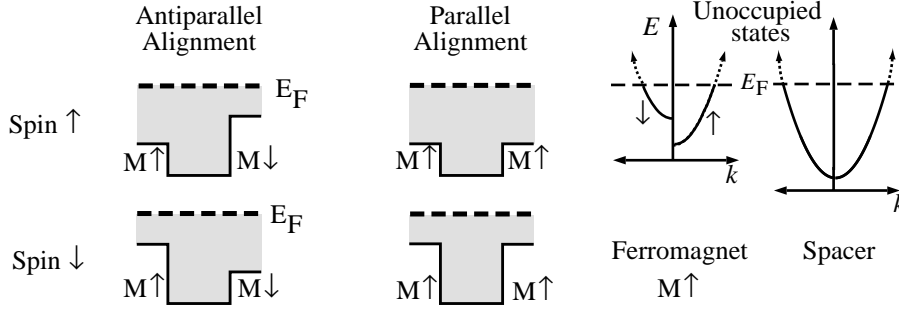


Figure 4: Quantum wells used to compute interlayer exchange coupling. On the right, the two panels give typical band structures for free electron models of interlayer exchange coupling. On the left, the four panels give the quantum wells for spin up and spin down electrons for parallel and antiparallel alignment of the magnetization. The gray regions designate the occupied states.

each can be computed separately. At this point, the calculation has been reduced to computing the single particle energies for the four quantum wells shown schematically in Fig. 4. The appropriate sums and differences of the energies give the interlayer exchange coupling.

For a simple trilayer, in which both ferromagnetic layers are semi-infinite, all the sums of single particle energies are infinite. However, the infinite contributions from the two ends cancel out. It is important to treat this cancellation correctly, which is most easily done by considering the “cohesive energy” of each quantum well. The cohesive energy is the energy required to make the quantum well out of its bulk constituent materials. For a quantum well with total ferromagnetic thickness  $L$  and spacer layer thickness  $D$  the cohesive energy is

$$\frac{\Delta E_{\text{qw}}}{A} = \frac{E_{\text{tot}}}{A} - L\epsilon_{\text{FM}} - D\epsilon_{\text{NM}}, \quad (4)$$

where  $\epsilon$  is the energy density of each bulk material that makes up the layers. When using the force theorem, the energy densities are just the single particle energy densities.

### 3.1 Quantum well states due to spin-polarized reflection

Electrons reflect from interfaces between two materials. For free electron models, the interface is a simple (spin-dependent) step in the potential and the reflection amplitudes are straightforward to compute. For real material interfaces, such a calculation is not so straightforward, but it is still feasible [73, 74, 75, 76].

In trilayers, electrons reflect from both interfaces and the multiply reflected waves interfere with each other. The amplitude for one round trip in a spacer layer of thickness  $D$  is  $e^{ikD} R_R e^{ikD} R_L$ , where  $e^{ikD}$  is the phase accumulated on one traversal of the spacer and  $R_{R/L}$  are the reflection amplitudes from the right and left interfaces. The amplitude for two round trips is the same quantity squared. For all possible round trips the total amplitude is

$$\sum_{n=1}^{\infty} [e^{i2kD} R_R R_L]^n = \frac{e^{i2kD} R_R R_L}{1 - e^{i2kD} R_R R_L}. \quad (5)$$

The denominator becomes small and there is constructive interference whenever  $2kD + \phi_R + \phi_L = 2n\pi$ , where  $n$  is an integer and  $\phi_{R/L} = \text{Im}[\ln(R_{R/L})]$  is the change in the phase of a reflected electron. The constructive interference inside the spacer layer gives rise to resonances, frequently referred to as quantum well states. Whenever the reflection probability is one, these quantum well states are true bound states. Otherwise they are like bound states that are broadened by transmission into the ferromagnetic layers. When the reflection amplitude is close to one,  $|R| \approx 1$ , the resonances are sharp and when the reflection amplitude is close to zero, they are broad. For a free electron model, these are shown schematically in Fig. 5.

As the thickness  $D$  of the spacer layer is varied, the resonances and bound states shift in energy. If there is a resonance at the Fermi energy at a thickness  $D$ , then resonances cross the Fermi energy whenever the thickness is  $D + 2n\pi/2k_F$ , where  $k_F$  is the Fermi wave vector of the spacer layer and  $n$  is an integer. This periodic crossing of the Fermi energy by quantum well resonances is the origin of the oscillations in the interlayer exchange coupling. In

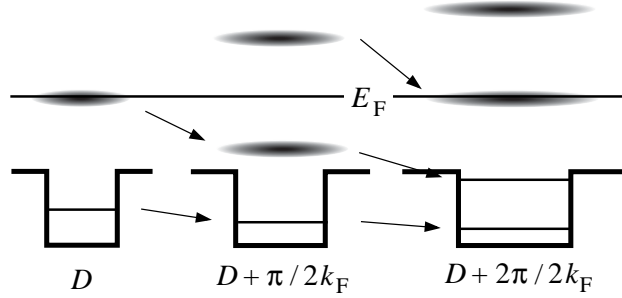


Figure 5: Evolution of quantum well resonances with spacer layer thickness. The three panels illustrate the bound states (lines) and resonances (fuzzy ellipses) for quantum wells of increasing thickness. The arrows indicate how each resonance evolves as the thickness is increased.

this 1-d model, the Fermi surface consists of two points,  $k = \pm k_F$ . The period is determined by the spanning vector of the Fermi surface,  $2k_F$ .

For closely related samples, these quantum well states have been seen in photoemission and inverse photoemission. For reviews, see [77, 78]. In these experiments, one of the ferromagnetic layers is left off so that the density of states in the spacer layer could be measured. Since the reflection amplitude from the surface is different from the interface with the ferromagnet, the resonances are sharper and slightly displaced in energy compared to the quantum well. Nevertheless, the peaks seen in the photoemission spectra of these samples show the expected behavior as a function of energy and thickness. In addition, the quantum well resonances seen in photoemission cross the Fermi level with the same periodicity as is found for the interlayer coupling in related trilayers. Since the reflection at the interface with the ferromagnetic layer is spin dependent, the quantum well states are spin dependent [79].

The quantum well states affect the density of states in trilayer, and hence the cohesive energy of the quantum well. The change in the density of states of the quantum well *for each spin*, defined similarly to the cohesive energy of the quantum well [14], is

$$\Delta n(E, D) = -\frac{1}{\pi} \text{Im} \left[ \frac{d}{dE} \ln (1 - e^{i2kD} R_R R_L) \right]. \quad (6)$$

The derivative of the  $\ln$  gives a factor that is the multiple scattering amplitude in the quantum well, Eq. (5). The cohesive energy of the quantum well is the sum of the single particle energies or equivalently, the integral over the change in the density of states

$$\Delta E_{\text{qw}} = - \int_{-\infty}^{E_F} dE (E - E_F) \Delta n(E, D). \quad (7)$$

For the time being, this is a one-dimensional model, so there is no factor of the area. This expression can be integrated by parts to give

$$\Delta E_{\text{qw}} = \frac{1}{\pi} \text{Im} \int_{-\infty}^{E_F} dE \ln (1 - e^{i2kD} R_R R_L) \quad (8)$$

This result is valid for the case when there is only one state going in each direction in the spacer layer. For the more general case, see [66, 80].

For fixed thickness, the integrand in Eq. (8) oscillates rapidly through the energy dependence of  $k$ . All of these oscillations cancel out in the integration, except those close to the Fermi energy, where there is a sharp cut-off. The only contribution is from a range of states near  $E_F$  of width proportional to  $\hbar v_F / D$ , where  $v_F$  is the Fermi velocity. Over this energy range, the energy dependence of  $R_{R/L}$  can be ignored and the wave vector can be assumed to vary linearly with energy,  $k \approx k_F + E / (\hbar v_F)$ , so that in the limit of a thick spacer layer

$$\lim_{D \rightarrow \infty} \Delta E_{\text{qw}} = \frac{\hbar v_F}{2\pi D} \sum_n \frac{1}{n} \text{Re} [(R_R R_L)^n e^{i2k_F n D}]. \quad (9)$$

Including the full energy dependence gives terms with higher order in  $D^{-1}$ , called preasymptotic corrections [81, 82]. When the reflection amplitudes are small only the first term in the sum over  $n$  contributes, giving

$$\lim_{D \rightarrow \infty} \Delta E_{\text{qw}} \approx \frac{\hbar v_{\text{F}}}{2\pi D} |R_{\text{R}} R_{\text{L}}| \cos [2k_{\text{F}} D + \phi_{\text{R}} + \phi_{\text{L}}]. \quad (10)$$

The higher powers of the reflection amplitudes give higher harmonics of the oscillation. They change the shape and weakly change the amplitude without changing the period. In the asymptotic limit, the cohesive energy for this one-dimensional model decays like one over the spacer-layer thickness, and oscillates with a period set by the (one-dimensional) Fermi spanning vector  $2k_{\text{F}}$  with a strength that goes like the product of the two reflection amplitudes. The cohesive energy decays because the energy range of states that contribute without cancellation decreases as  $\hbar v_{\text{F}}/D$ .

The interlayer exchange coupling is then the sum and difference of the cohesive energies for the four different quantum wells seen in Fig. 4. All four quantum wells have cohesive energies that oscillate with the same period because their oscillation period is determined by the Fermi surface spanning vector of the spacer layer material. The oscillations do not cancel because they have different amplitudes and possibly phases. For this one-dimensional case, in the large  $D$ , small  $R$  limit, the result is

$$\begin{aligned} \lim_{D \rightarrow \infty} J &\approx \frac{\hbar v_{\text{F}}}{4\pi D} \text{Re} [(R_{\uparrow} R_{\downarrow} + R_{\downarrow} R_{\uparrow} - R_{\uparrow}^2 - R_{\downarrow}^2) e^{i2k_{\text{F}} D}] \\ &\approx -\frac{\hbar v_{\text{F}}}{4\pi D} \text{Re} [(R_{\uparrow} - R_{\downarrow})^2 e^{i2k_{\text{F}} D}]. \end{aligned} \quad (11)$$

Here, I have assumed that the reflection amplitudes are the same for the left and right interfaces but they depend on whether the spin is majority ( $\uparrow$ ) or minority ( $\downarrow$ ). The first form above shows the contribution for each of the quantum wells, the two asymmetric quantum wells for antiparallel alignment of the magnetizations minus the majority and minority quantum wells for parallel alignment. The second form shows that the interlayer exchange coupling depends on the spin dependence of the reflection amplitudes.

### 3.2 Critical spanning vectors

Real multilayers are three dimensional, not one dimensional. However, if the interface is coherent and there are no defects, the multilayer is periodic in the two directions parallel to the interface. Then, the crystal momentum parallel to the interface,  $\mathbf{K}$ , is conserved. In this case, the problem simplifies to a two-dimensional set of *independent* one-dimensional quantum wells. This simplification is the reason that all (to my knowledge) theoretical treatments of interlayer exchange coupling assume coherent interfaces. For an ideal interface, the cohesive energy (now per area) is just the integral over the interface Brillouin zone (IBZ) of a series of one-dimensional quantum well energies.

$$\frac{\Delta E_{\text{qw}}}{A} = \frac{1}{\pi} \int_{\text{IBZ}} \frac{d^2 K}{(2\pi)^2} \text{Im} \int_{-\infty}^{E_{\text{F}}} dE \ln \left( 1 - e^{i2k_z(\mathbf{K})D} R_{\text{R}}(\mathbf{K}) R_{\text{L}}(\mathbf{K}) \right) \quad (12)$$

In the small  $R$ , large  $D$  limits, integrating over energy as above gives

$$\lim_{D \rightarrow \infty} \frac{\Delta E_{\text{qw}}}{A} \approx \frac{\hbar v_{\text{F}}}{2\pi D} \int_{\text{IBZ}} \frac{d^2 K}{(2\pi)^2} \text{Re} \left( e^{i2k_{\text{F}_z}(\mathbf{K})D} R_{\text{R}}(\mathbf{K}) R_{\text{L}}(\mathbf{K}) \right). \quad (13)$$

Each parallel wave vector has a different one-dimensional Fermi surface given by  $k_{\text{F}_z}(\mathbf{K})$ . For each parallel wave vector, the energy integration gives an oscillation as a function of thickness with a period set by its Fermi surface spanning vector,  $2k_{\text{F}_z}(\mathbf{K})$ .

For large  $D$ , the integrand oscillates rapidly as a function of  $\mathbf{K}$ , through the  $\mathbf{K}$  dependence of  $2k_{\text{F}_z}(\mathbf{K})$ . As is the case above for the energy integration, the oscillations all tend to cancel out, except where there is a sharp cut-off. For the parallel wave vector integration, these cut-offs occur where two sheets of the Fermi surface become parallel in the direction of the interface normal, see Fig. 1. The vector connecting the two parallel points is called a critical spanning vector. The projection into the interface Brillouin zone of the points where the Fermi surface sheets become parallel is called the critical point. The regions of the Fermi surface close to the critical point have oscillations that

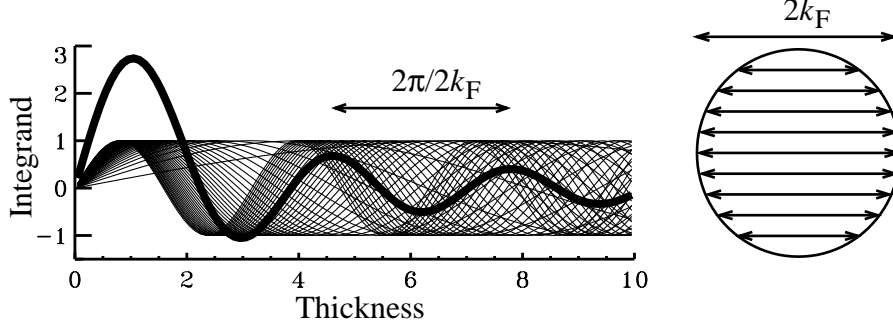


Figure 6: Selection of critical spanning vectors. The right panel shows a slice through a free electron Fermi surface and some spanning vectors. The left panel shows the oscillating functions from each of these spanning vectors (light curves) and the integral over all of them (heavy curve). The peaks in the heavy curve come from constructive interference among some of the light curves. Fewer and fewer of the light curves interfere constructively as the thickness increases.

contribute in phase with each other, see Fig. 6. As the spacer layer thickness increases, the area of the Fermi surface that contributes in phase decreases as  $\kappa/D$ , where  $\kappa$  is the radius of curvature of the Fermi surface at the critical point. This behavior gives an additional factor of  $D^{-1}$  to the decay of the cohesive energy.

For thick spacer layers, the  $\mathbf{K}$  dependence of the reflection amplitudes is ignored and the  $\mathbf{K}$  dependence of  $k_z$  is expanded to quadratic order. The Fermi surface spanning vectors,  $q$  close to the critical point satisfy

$$q = 2k_F + \frac{1}{\kappa_u}k_u^2 + \frac{1}{\kappa_v}k_v^2 \quad (14)$$

where  $u$  and  $v$  are the principle axes of this paraboloid. For simplicity, I have taken the critical point to be at the center of the Interface Brillouin zone. In the large  $D$  limit, the parallel wave vector integration in Eq. (13), reduces to the form

$$\int_{-\infty}^{\infty} dx \int_{-\infty}^{\infty} dy e^{i(\frac{x^2}{a} + \frac{y^2}{b} + c)} = \pi e^{ic} \sqrt{|ab|} e^{ix}. \quad (15)$$

The final factor is  $e^{ix} = i, 1, -i$  for local minima ( $a > 0$  and  $b > 0$ ), saddle points ( $ab < 0$ ), and maxima ( $a < 0$  and  $b < 0$ ) respectively. Equation (13) becomes

$$\lim_{D \rightarrow \infty} \frac{\Delta E_{qW}}{A} \approx \frac{\hbar v_F \kappa}{8\pi^2 D^2} \text{Re} [R_R R_L e^{i2k_F D} e^{ix}], \quad (16)$$

where  $\kappa = \sqrt{|\kappa_u \kappa_v|}$  is the average radius of curvature of the Fermi surface difference at the critical point. For a free electron Fermi surface it is just  $k_F$ . Including the  $\mathbf{k}$  dependence of the reflection amplitudes and higher order terms in the expansion of  $q$  gives terms in the cohesive energy that decay as higher powers of  $D^{-1}$ . These are additional preasymptotic corrections [82].

### 3.3 Asymptotic form

Each critical spanning vector makes a contribution to the cohesive energy as in Eq. (16). The contributions from each quantum well in Fig. 4 are added and subtracted to give the interlayer exchange coupling. With the critical spanning vectors indexed by  $\alpha$ , the interlayer exchange coupling takes its asymptotic form

$$\begin{aligned} \lim_{D \rightarrow \infty} J(D) &\approx \sum_{\alpha} \frac{J^{\alpha}}{D^2} \sin(q_{\perp}^{\alpha} D + \phi^{\alpha}) \\ &\approx \sum_{\alpha} \frac{\hbar v_{\perp}^{\alpha} \kappa^{\alpha}}{16\pi^2 D^2} \text{Re} [(R_{\uparrow}^{\alpha} - R_{\downarrow}^{\alpha})^2 e^{iq_{\perp}^{\alpha} D} e^{ix^{\alpha}}]. \end{aligned} \quad (17)$$

Interface	Period (ML)	Period (ML)	Technique	Reference
Ag/Fe(100)	2.38	5.58	dHvA	[40]
	$2.37 \pm 0.07$	$5.73 \pm 0.05$	SEMPA	[86]
Au/Fe(100)	2.51	8.60	dHvA	[40]
	$2.48 \pm 0.05$	$8.6 \pm 0.3$	SEMPA	[7]
Cu/Co(100)	2.56	5.88	dHvA	[40]
	$2.60 \pm 0.05$	$8.0 \pm 0.5$	MOKE	[23]
	2.58 to 2.77	6.0 to 6.17	SEMPA	[87]
Cr/Fe(100)	11.1		dHvA	[88, 89]
	$12 \pm 1$		SEMPA	[25]
	12.5		MOKE	[90]
Cr/Fe(112)	14.4		dHvA	[88]
	15.4		MOKE	[90]

Table 1: Comparison of oscillation periods measured in magnetic multilayers with those expected from the critical spanning extracted from Fermi surfaces measured in de Haas-van Alphen measurements (dHvA).

where  $q_{\perp}^{\alpha}$  is the length of the critical spanning vector,  $e^{ix^{\alpha}}$  is the phase from the type of critical point (maximum, minimum, saddle point), and  $\phi^{\alpha}$  is a phase determined by  $\chi^{\alpha}$  and the phases of the reflection amplitudes. The effective Fermi velocity is defined as

$$\frac{2}{v_{\perp}^{\alpha}} = \frac{1}{|v_{F\perp}^r|} + \frac{1}{|v_{F\perp}^l|}, \quad (18)$$

where  $v_{F\perp}^{r/l}$  are the components of the Fermi velocities in the interface direction for the right and left going states at the critical point. Equation (17) differs by factors of two from other versions of the same result. These factors depend on the definition of  $J$ , Eq. (1), and the definitions of  $v_{\perp}^{\alpha}$  and  $\kappa^{\alpha}$ . Here, the latter two have been chosen so that they reduce to  $v_F$  and  $k_F$  for free electron models. Also, in some versions the difference in the reflection amplitudes is written  $\Delta R = (R_{\uparrow} - R_{\downarrow})/2$ , which introduces additional factors of two.

The asymptotic form, Eq. (17) is the main result of this model. In common with previous models, it shows that the oscillation periods of the interlayer exchange coupling are determined by the critical spanning vectors of the Fermi surface. This model shows that the strength of the oscillation for each critical spanning vector is determined by properties of the spacer layer Fermi surface,  $v_{\perp}^{\alpha}$ , and  $\kappa^{\alpha}$ , and by the spin difference in the reflection amplitudes. In the context of this result, other models can be interpreted as different approximations for the reflection amplitudes. In RKKY models, the reflection amplitudes depend on the spin-dependent scattering by the localized impurities. In infinite- $U$  models, the reflection amplitudes are either zero or one. In free electron models, they are determined by scattering from potential steps.

Generally speaking, the reflection amplitudes in Eq. (17) are the reflection amplitudes for all of the material on either side of the the spacer layer. Thus, if the ferromagnetic layers have a finite thickness, they should be the reflection amplitudes for a finite thickness of the ferromagnet. If there is a capping layer, it affects the reflection amplitudes as well. If the outer surfaces of the ferromagnetic layers are flat enough, there are resonances in the ferromagnet (and capping layer) that cause the coupling to oscillate. Both have been seen experimentally [83, 84, 85]. Different ferromagnetic layers, e.g. different thicknesses, can lead to differences between theoretical results and between theoretical and experimental results.

When spacer layers adopt their bulk structure, their critical spanning vectors can be determined from the Fermi surfaces that have been measured by de Haas-van Alphen experiments, as shown in Table 1. When compared with periods determined from high precision measurements of wedge-shaped spacer layers with SEMPA, the agreement is quite remarkable. The comparison of results for the long period of Cu(001) spacer layers is not as good as other results. Possible reasons for this are discussed below. For the Cr spacer layer, the entries in the Table are only for the long period. The periods extracted from the de Haas-van Alphen measurements for Cr are for the Fermi surface pocket centered at the  $N$ -point in the Brillouin zone. Justification for this choice, in addition to the *a posteriori* agreement in the Table, is discussed below.

While the agreement between the measured periods and the experimental Fermi surface properties is quite good, the agreement between measured and calculated coupling strengths is not as good. I discuss several examples in Sec. 5.

There are several reasons for the lack of agreement. On the experimental side, the oscillation periods are not affected by disorder to lowest order, but the oscillation amplitudes are. Also, the highest precision measurements of the periodicity were made with SEMPA on wedge-shaped samples. Since SEMPA is generally not compatible with applied fields, SEMPA has not been used to measure coupling strengths. On the theoretical side, the experimentally measured Fermi surfaces are not sufficient to compute the coupling strengths. There remain two theoretical approaches, both of which have disadvantages. One approach is to go back to Eq. (3) and compute the total energies using the LSDA or a tight-binding approach. The other approach is to compute the coupling strengths using Eq. (17) by calculating the spin-dependent reflection amplitudes for realistic band structures. Such calculations also require the LSDA or a tight-binding approach.

Formally, the LSDA is justified for computing total energies of different configurations, but not for computing band structures or related quantities like reflection amplitudes. However, to study interlayer exchange coupling it is useful to view LSDA as a single-particle approximation that treats the electron-electron interaction in mean field theory. In this approach, LSDA does a good, but imperfect, job of predicting band structures for transition metals. However, this approach makes it possible to connect the total energy calculations with the model calculations. Hopefully, the discussion of the model has made it clear that the properties of the LSDA band structure (even though it may not be formally justified) determine the results of the total energy calculations.

The differences between real Fermi surfaces and those calculated using the LSDA complicate the comparison between theory and experiment. The results from total energy calculations cannot be compared directly to experiment because the underlying Fermi surface gives oscillation periods that are at least slightly off. After several oscillations, theory and experiment become out of phase and impossible to compare. On the other hand, very few measurements are made for films thick enough that the asymptotic limit is reached. Comparison with the asymptotic results is difficult when preasymptotic corrections are important.

### 3.4 Disorder

All measurements are made at finite temperature,  $T$ . A number of calculations [50, 67] have shown that the effect of a thermal electron distribution in the spacer layer is to multiply each term in the asymptotic form, Eq. (17), by the factor

$$\frac{2\pi k_B T D / (\hbar v_{\perp}^{\alpha})}{\sinh [2\pi k_B T D / (\hbar v_{\perp}^{\alpha})]}. \quad (19)$$

For a typical free electron Fermi velocity ( $1.5 \times 10^{15}$  nm/s) and a spacer thickness of  $D = 4$  nm, Eq. (19) is approximately 0.998 at room temperature (compared to 1 at zero temperature) and can frequently be ignored. This correction accounts for the temperature dependence of the electrons in the spacer layer, but not the temperature dependence of the ferromagnetic layers. The low-lying excitations of a ferromagnet are spin waves, which correspond to time-dependent local rotations in the direction of the magnetization rather than its value. These rotations change the relative orientation of the magnetizations on either side of the interface and hence change the net coupling between them [91]. However, in most measurements, the measurement temperature is significantly below the Curie temperature so there is not much spin wave excitation. Thus, it is often a good approximation to ignore the temperature dependence of the bilinear coupling.

The simplest type of disorder to treat is the effect of thickness fluctuations. In many samples the spacing between steps at the interfaces is in an intermediate regime. The spacing is large enough that the description of the coupling for ideal interfaces holds for the regions between the steps. At the same time, it is small enough compared to the intralayer domain wall widths in the ferromagnetic layers that the magnetization directions do not rotate significantly between steps. The consequence of this slight rotation – biquadratic coupling – is discussed in Sec. 4. In this regime, the effective bilinear coupling is given by the average of the couplings over the different thicknesses present in the spacer layer. If the coupling for an ideal thickness of  $n$  layers of thickness  $D_0$  is  $J(n)$  and the probability of having a thickness  $nD_0$  for a nominal deposited thickness of  $D$  is  $P(n, D)$ , the effective coupling strength is

$$J(D) = \sum_n P(n, D) J(n). \quad (20)$$

If the width of the growth front is measured by scanning tunneling microscopy, x-ray diffraction or some other technique, theoretical coupling strengths can be averaged to compare with measured strengths.

Steps are not only associated with thickness fluctuations, they are also scattering centers that cause diffuse scattering, see Fig. 7. Steps are one type of interfacial defect, other types are dislocations that form to relieve

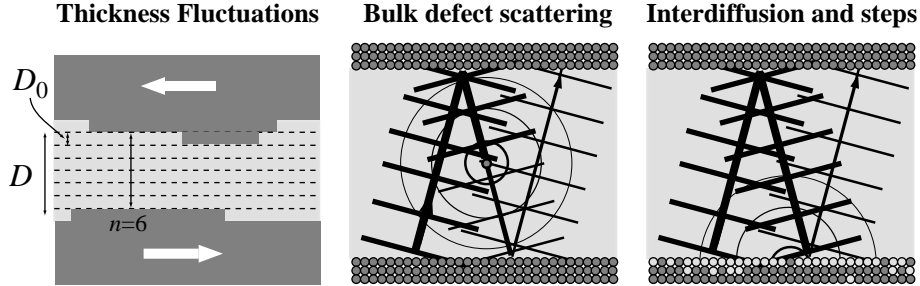


Figure 7: Schematic types of disorder. The left panel shows a multilayer with thickness fluctuations in the spacer layer. Several thicknesses are indicated,  $D_0$  is the thickness of an individual layer,  $D = 6.5 D_0$  is the average thickness of the spacer layer, and  $n = 6$  is the number of layers at one point. The middle panel shows an electron wave reflecting from both interfaces. Scattering from a bulk defect reduces the amplitude, reducing the interference and hence the amplitude of the quantum well state. The right panel shows a similar process for a defect located at one of the interfaces.

heteroepitaxial stress and interdiffused atoms. The effect of localized interdiffusion has been studied [92, 93, 94, 95, 96, 97], but, to my knowledge, the effect of extended defects, like steps and dislocations has not. Calculations that treat interfacial disorder typically use either a periodic array of defects or the coherent potential approximation.

Inspection of the asymptotic formula, Eq. (17) can give a qualitative understanding of the effects of interdiffusion and defect scattering. When the interdiffusion is localized to the interface, the properties of the spacer layer do not change, so only the reflection amplitudes are changed. If the interdiffused atoms are far apart, they mainly contribute to the incoherent scattering at the expense of the coherent scattering. This process reduces the reflection amplitudes. The reduction can depend strongly on spin [98] and even on which part of the Fermi surface is involved [96]. As the intermixing becomes greater, the interface starts to behave more like an averaged material and the incoherent scattering from each defect can decrease. Bulk defects, on the other hand, affect the properties of the spacer layer, and not the reflection amplitudes (at least to a first approximation). In the asymptotic formula, Eq. (17), the effect of bulk scattering could be modeled by adding an imaginary part to the critical spanning vector. The imaginary part comes from the reduction of the coherent part of the wave function due to incoherent scattering. One consequence of incoherent scattering of either type is to reduce the importance of multiple trips through the spacer and hence make the higher harmonics neglected in Eq. (10) less important.

The only type of bulk defect that has been treated theoretically is alloying in the spacer layer. The effect of the defect scattering due to the alloying is usually of secondary interest. The main focus of these studies is to systematically vary the electronic structure, and hence critical spanning vectors, of the spacer layer to develop a better understanding of the coupling. Comparison between measurements [52, 99, 100, 101, 102, 103] and calculations [101, 102, 103, 104, 105] of the variation of the coupling periods as a function of composition gives evidence as to the origin of the coupling. I discuss this point more below for the case of Fe/Cr.

## 4 Other coupling mechanisms

The behavior of magnetic multilayers can be controlled by other coupling mechanisms besides the bilinear coupling discussed above. Of these, the most important are various forms of biquadratic coupling, Eq. (2). This section focuses on the various extrinsic sources of biquadratic coupling. It also touches on other extrinsic coupling mechanisms.

There is an intrinsic source of biquadratic coupling that is directly related to the bilinear coupling [106, 107, 108]. Computing the full dependence on  $\hat{\mathbf{m}}_1 \cdot \hat{\mathbf{m}}_2$  of the model discussed in Section 3 rather than just the endpoints,  $\hat{\mathbf{m}}_1 \cdot \hat{\mathbf{m}}_2 = \pm 1$ , reveals that the coupling depends on higher orders of the angle between the magnetizations. It turns out however, that the higher order terms are much smaller than the bilinear term,  $n = 1$ , and are generally negligible. Further, the biquadratic contribution that comes from this expansion oscillates between favoring collinear and perpendicular alignment of the magnetizations. In experiment, biquadratic coupling appears to always favor perpendicular alignment. This discrepancy, and the small size of the intrinsic biquadratic coupling argue in favor of an extrinsic origin for observed biquadratic coupling.

## 4.1 Thickness-fluctuation biquadratic coupling

Typically, intralayer exchange coupling prevents the magnetization direction in the ferromagnetic layers from rotating too rapidly in space. Thus, in the presence of variations in the spacer layer thickness, the bilinear coupling gets averaged over the growth front as described in Eq. (20). However, the intralayer exchange is not infinite. The finite intralayer exchange coupling gives a second consequence of thickness variations – biquadratic coupling.

In this section, I present a version of the result due originally to Slonczewski [11, 33] demonstrating the generation of biquadratic coupling by thickness variations. The basic idea is quite simple. The biquadratic coupling is an effective coupling due to fluctuations in the layer magnetizations around their average directions. There are regions of the multilayer with different coupling strengths (due to different thicknesses). Since the intralayer exchange coupling is strong enough that the layers each have well-defined average magnetization directions, each average direction is determined by the coupling, the external field, and whatever anisotropies are present. With the average directions so determined, regions where the coupling would tend towards greater alignment between the magnetizations balance the regions where the coupling would tend towards less alignment. However, the intralayer exchange coupling is not so strong that the system cannot lower its energy by allowing the magnetization in each region to rotate slightly away from the average towards its preferred direction. It turns out that these fluctuations give the greatest energy gain when the magnetizations are perpendicular and no gain when they are collinear. Thus, these fluctuations give an effective interaction between the average magnetization directions that favors perpendicular alignment of the average directions.

In the presence of thickness variations, the interlayer exchange coupling  $J(\mathbf{R})$  depends on the position  $\mathbf{R}$  in the plane of the interface. The average bilinear coupling is the average of the local bilinear coupling

$$J_1 = \frac{1}{A} \int d^2R J(\mathbf{R}), \quad (21)$$

where  $A$  is the area. The variations in the coupling give an effective biquadratic coupling between the average magnetizations with the strength [109]

$$J_2 = -\frac{1}{4A} \int \frac{d^2K}{(2\pi)^2} \frac{J(\mathbf{K})J(-\mathbf{K})}{A_{\text{ex}}K}, \quad (22)$$

where  $A_{\text{ex}}$  is the intralayer exchange coupling constant,  $K = |\mathbf{K}|$ , and  $J(\mathbf{K})$  is the Fourier transform of the interlayer exchange coupling constant

$$J(\mathbf{K}) = \int d^2R e^{i\mathbf{K}\cdot\mathbf{R}} (J(\mathbf{R}) - J_1). \quad (23)$$

Equation (22) can be more easily understood in simple limits.

Consider the simple model in which the spacer layer consists of parallel strips of width  $L$  with alternating thicknesses and hence coupling strengths  $J^n$  and  $J^{n+1}$ , see Fig. 8. For this model, the relative angle of the magnetizations is  $\theta = \theta_0 + \delta\theta \sin(\pi x/L)$ , where  $\delta\theta$  is the size of the fluctuations. Over the region from 0 to  $L$ , where the coupling is  $J^n$ , the energy change due to the fluctuations is proportional to  $J^n \delta\theta$ . Over the region from  $L$  to  $2L$ , the sine function changes sign and the energy change due to the fluctuations is proportional to  $-J^{n+1} \delta\theta$ . The net coupling energy per area due to the fluctuations is proportional to  $-\delta J \delta\theta$ , where  $\delta J = J^n - J^{n+1}$ . Fluctuations in the right direction lower the energy of the system. The energy gain is balanced by the cost in intralayer exchange energy because the magnetization now varies spatially. Since the intralayer exchange coupling depends on the square of the gradient of the magnetization, for this simple model, it is proportional to  $(A_{\text{ex}}/L) \delta\theta^2$ . Combining the changes due to the fluctuations for the interlayer exchange coupling and the intralayer exchange and finding the minimum with respect to the amplitude of the fluctuations gives  $\delta\theta \propto -\delta J / (A_{\text{ex}}/L)$ . For this fluctuation amplitude, the change in the energy per area due to the fluctuations gives the strength of the biquadratic coupling

$$J_2 \sim -\frac{(\delta J)^2 L}{A_{\text{ex}}}. \quad (24)$$

This form is also found from (22) by inserting the specific form of  $J(\mathbf{R})$ .

While (24) is quite simple, its qualitative features generalize to more realistic situations. In real systems, the stripes are replaced by arbitrary-shaped terraces of different thicknesses, still, there is usually a characteristic length

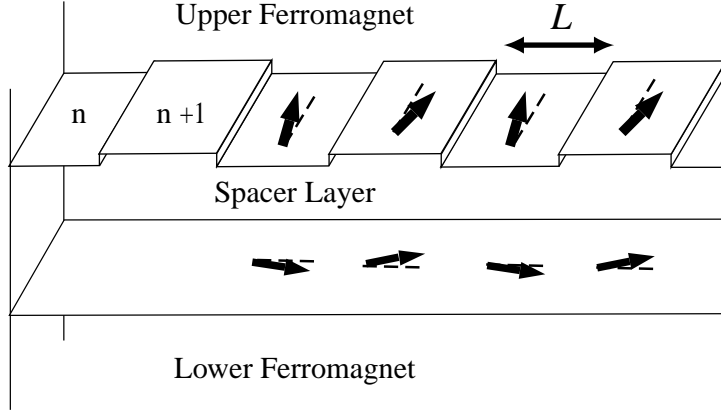


Figure 8: Thickness variations and biquadratic coupling. For a trilayer in which the thickness of the spacer layer varies periodically between  $n$  and  $n + 1$  layers, the heavy arrows show the local variation in the magnetization direction. In the regions with an  $n$ -layer thick spacer, in which the coupling is taken to be antiferromagnetic, the magnetizations rotate a little away from each other. For the  $n + 1$ -layer thick regions, in which the coupling is taken to be ferromagnetic, they rotate toward each other.

scale  $L$  that determines the biquadratic coupling. The biquadratic coupling strength increases when this length scale increases because the fluctuations can get larger. However, if the terraces get too large, the fluctuations get large enough that the average direction loses its meaning. Also, more than two thicknesses are generally present in the growth front, but that just introduces an effective  $\Delta J$ . The coupling increases as the difference in the coupling for the different terraces get larger. The differences tend to be largest when the coupling is oscillating rapidly, that is when there is short period coupling. The coupling gets weaker as the intralayer exchange interaction increases because exchange suppresses the fluctuations in magnetization direction that lower the energy.

The form for the biquadratic coupling in Eq. (22) has been derived for semi-infinite ferromagnetic layers. In the opposite limit, in which the thicknesses of the upper and lower ferromagnetic layers,  $t_{U/L}$ , are thinner than the length scale of the important fluctuations,  $L$ , an additional factor of  $K^{-1}(t_U^{-1} + t_L^{-1})/2$  should be included in the integrand of the coefficient of the biquadratic coupling. The biquadratic coupling gets stronger as the films become thinner because the exchange-energy penalty gets smaller, allowing the fluctuations to get larger. In this limit, the result for the simple model, Eq. (24) gets an additional factor of  $(L/t_U) + (L/t_L)$ .

While short period oscillations in the bilinear coupling favor the generation of biquadratic coupling, short period coupling is not necessary. In fact, the bilinear coupling does not even need to change sign to give a biquadratic contribution to the coupling. This last point may seem surprising, because on first glance it does not appear that there is any frustration in the system. However, when the applied field is such that the magnetizations are not collinear, there is still a balance between regions that would rotate closer to perpendicular and those that would rotate further away.

Finally, to be in the limit that the average magnetization direction is well defined, the biquadratic coupling must be weaker than the absolute value of the unaveraged bilinear coupling. However, the biquadratic coupling can be stronger than the *averaged* bilinear coupling when couplings of different sign are present in the growth front, because the effective bilinear coupling is averaged over the growth front.

Strong evidence for this mechanism of biquadratic coupling comes from wedged Cr spacer layers on Fe whiskers [110]. Cr has a short period bilinear coupling that is almost commensurate with the lattice. There is a node in the short period coupling when the number of layers is  $n_0 \approx 24$  where the coupling strength behaves roughly like  $J_n \sim (n - n_0)(-1)^n$  [30, 110]. In samples that show these short period oscillations, regions of parallel alignment are separated from regions of antiparallel alignment by regions of perpendicular alignment. If we assume perfect layer by layer growth, the average bilinear coupling varies linearly between complete layers. Somewhere between the two thicknesses of complete layers the coupling goes through zero. Near this thickness, the biquadratic coupling dominates the averaged bilinear coupling. The width of this region is roughly determined by the strength of the biquadratic coupling at the halfway point divided by the slope of the linearly varying bilinear coupling. For bilinear coupling that goes to zero near the node, the width of the biquadratically coupled regions goes to zero linearly around

the node in the coupling,  $W \sim |n - n_0|$ .

If the sample is grown at a lower temperature, the thickness fluctuations are greater and the short period bilinear coupling is obscured. A long period coupling reveals itself. In the regions where the long period coupling goes through zero, the average bilinear coupling also varies linearly, but with a slope that is not related to the short period coupling. In this case, the width of the transition region goes to zero quadratically near the node in the otherwise obscured bilinear coupling,  $W \sim (n - n_0)^2$ . Within experimental uncertainty, both the linear and quadratic variation of the transition widths are observed in the appropriate samples [110].

## 4.2 Pin-hole coupling

The simplest coupling that competes with the interlayer exchange coupling is the coupling due to the presence of pinholes. A pinhole, in this context, is a break in the spacer layer giving direct exchange coupling between the two ferromagnetic layers. Since there is direct contact between the ferromagnetic layers, pin-hole coupling is ferromagnetic. Historically, early attempts to separate ferromagnetic layers by a non-magnetic layer were frustrated by the presence of pinholes. It was the observation of antiferromagnetic coupling in 1986 [1] that gave convincing evidence that some coupling besides pin-holes was dominant. Even when pin-hole coupling does not dominate the bilinear coupling, it can cause biquadratic coupling when the bilinear coupling is antiferromagnetic [111]. This mechanism is closely related to the thickness-fluctuation-induced biquadratic coupling, but requires an appropriate distribution of pinholes rather than a distribution of thicknesses with appropriate couplings.

## 4.3 Magnetostatic coupling

Magnetostatic interactions make two types of contributions to the properties of magnetic multilayers, macroscopic and microscopic. The main macroscopic contribution is a demagnetizing factor that gives a strong anisotropy to keep the magnetizations in plane. Since other macroscopic magnetostatic effects are negligible on thin film samples, all macroscopic magnetostatic effects are typically replaced by an effective uniaxial anisotropy that pushes the moments in plane. On the other hand, in patterned thin film samples, with reduced lateral dimensions, the macroscopic magnetostatic interactions can become quite important.

There are two coupling mechanisms that arise from magnetostatic interactions on a microscopic scale. Both are related to the roughness of the thin films. A ferromagnetic coupling, originally described by Néel [112], is frequently called “orange peel” coupling [113, 114, 115, 116, 117]. More recently, Demokritov et al. [118] demonstrated that roughness and magnetostatic interactions can give a biquadratic coupling. Both of these couplings come from the fringing fields that exist outside the surface due to roughness.

When a surface is rough, there are magnetic poles at the surface because the intralayer exchange is strong enough to prevent the magnetization from rotating and following the surface profile. A useful limit, at least from a pedagogical point of view, is where the roughness of the interfaces is slowly varying and much smaller in amplitude than the separation of the interfaces. Slowly varying implies that the local surface normal is always close to the average surface normal. Then, it is possible to replace the magnetostatics of the rough interfaces by a distribution of magnetic “charges” on a flat surface

$$\sigma(\mathbf{R}) = \mathbf{M} \cdot \mathbf{n}(\mathbf{R}). \quad (25)$$

Here, the magnetization  $\mathbf{M}$  is assumed to be uniform, and the local normal to the interface  $\mathbf{n}$  varies with local (two-dimensional) position  $\mathbf{R}$  on the surface. This surface charge density describes a flat approximation for a rough interface. By analogy with electrostatics, the interaction between two such interfaces separated by a non-magnetic spacer layer of thickness  $D$  is

$$E = \mu_0 \int d^2 R \int d^2 R' \frac{\sigma_U(\mathbf{R})\sigma_L(\mathbf{R}')}{\sqrt{D^2 + (\mathbf{R} - \mathbf{R}')^2}}, \quad (26)$$

where U(L) denotes the upper (lower) interface. Orange peel coupling arises in situations where the spacer layer has a uniform thickness. In this case, frequently described as having conformal or correlated roughness, the interface normals are locally opposite,  $\mathbf{n}_U = -\mathbf{n}_L = \mathbf{n}$ . When there is no preferred direction to the roughness, the interaction becomes [109]

$$J_1 = \frac{\mu_0 M_s^2}{4\pi} \int d^2 K |\mathbf{n}_\perp(\mathbf{K})|^2 \frac{e^{-KD}}{K}. \quad (27)$$

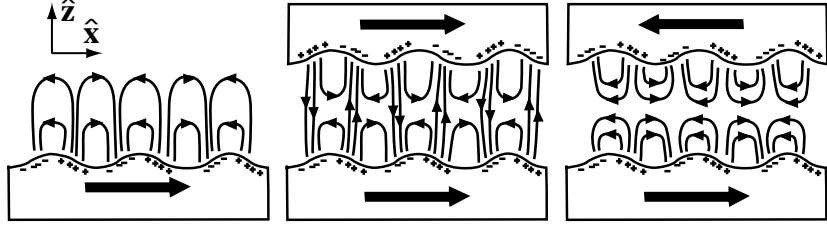


Figure 9: Orange peel coupling from correlated roughness. The left panel shows the fringing field outside a rough surface of a material with a uniform magnetization. The pluses and minuses are the effective magnetic “charges.” The middle panel shows how the fringing fields change in the presence of another interface with correlated roughness for the case of parallel magnetizations. The right panels shows that for antiparallel magnetizations, none of the field lines cross the center line, raising the field energy.

where  $\mathbf{n}_\perp(\mathbf{K})$  is the Fourier transform of the part of the local normal that is transverse to the average normal. Since the magnetizations are assumed to be in-plane, only the transverse component contributes. This bilinear coupling is the orange-peel coupling described by Néel.

Equation (27) can be made more intuitive by considering the case of sinusoidally varying interfaces,  $z_L = \delta \cos(2\pi x/L)$  and  $z_U = D + \delta \cos(2\pi x/L)$ , see Fig. 9. When the magnetization in one layer is perpendicular to the corrugation, i.e. along  $\hat{\mathbf{x}}$  in this case, there is ferromagnetic coupling to the other layer with strength

$$J_1 \sim \mu_0 M_s^2 \frac{\delta^2}{L} e^{-2\pi D/L}. \quad (28)$$

When the magnetization in one layer is along the corrugation, i.e. along  $\hat{\mathbf{y}}$ , rather than perpendicular, there is no coupling to the other layer. The dependence on the absolute directions of the magnetizations, rather than just the relative orientation is a consequence of directionality of the roughness in this simple model. Fully isotropic roughness gives a true ferromagnetic bilinear coupling. Since this coupling depends exponentially on the thickness of the spacer layer, the dominant roughness will tend to have periods somewhat greater than the spacer layer thickness. As the roughness increases, the coupling energy increases quadratically, just as the electrostatic interaction between two equal charges increases as the square of the charges. Both the general expression and the model result break down when the thickness of the spacer layer goes to zero because the roughness is no longer small compared to the spacer layer thickness.

When the roughness is uncorrelated, the orange-peel coupling is zero, but there is still a microscopic magnetostatic contribution to biquadratic coupling. In the limit that the magnetizations are uniform, the energy is independent of the relative magnetization directions when the roughness is uncorrelated and there is no coupling. However, when the intralayer exchange coupling is finite so that the magnetization directions can fluctuate, there will be biquadratic coupling. Above, I argued that when thickness fluctuations give spatial variations in the bilinear coupling, fluctuations in the magnetization direction can lower the energy. Here also, fluctuations in the magnetization direction can lower the energy. In both cases, the fluctuations lower the energy the most when the two magnetizations are nominally perpendicular.

Above a rough surface, magnetic charges give rise to a magnetic field which couples to the magnetization of the upper film. The magnetic field due to roughness in the lower interface is

$$\mathbf{B}(\mathbf{r}) = \mu_0 \int \frac{d^2 K}{(2\pi)^2} \frac{\mathbf{k}}{iK} e^{i\mathbf{K}\cdot\mathbf{R}} e^{-Kz} \int d^2 R' e^{-i\mathbf{K}\cdot\mathbf{R}'} \sigma_L(\mathbf{R}') \quad (29)$$

where  $\mathbf{K}$  is a two-dimensional wave vector in the plane of the interface and  $\mathbf{k} = (\mathbf{K}, i|\mathbf{K}|)$  is a complex three dimensional wave vector. The interaction between the rough lower layer and a semi-infinite upper layer is

$$E = - \int d^2 R \int_D^\infty dz \mathbf{M}_U(\mathbf{r}) \cdot \mathbf{B}_L(\mathbf{r}), \quad (30)$$

Note that this interaction is not between the charges on the two interfaces, but between the charges on one interface and the whole volume of the other layer. Responding to variations in  $\mathbf{B}_L(\mathbf{r})$ , fluctuations in  $\mathbf{M}_U(\mathbf{r})$  lower the

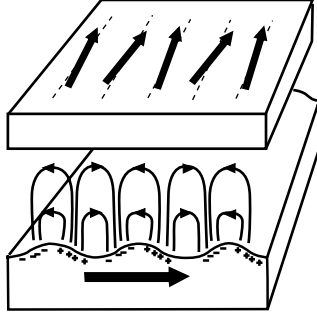


Figure 10: Biquadratic coupling from uncorrelated roughness. The fringing fields from the bottom, corrugated surface couple to the perpendicular magnetization in the smooth upper layer giving small amplitude oscillations in the magnetization direction.

magnetostatic energy at the expense of raising the exchange energy. The net lowering of the energy due to the fluctuations is greatest when the magnetizations are perpendicular. Assuming that the roughness has no preferred direction, the resulting biquadratic coupling has the form [109]

$$J_2 = -\frac{\mu_0^2 M_s^4}{64 A_{\text{ex}} A} \int \frac{d^2 K}{(2\pi)^2} \frac{e^{-2KD}}{K^3} |\mathbf{n}_\perp(\mathbf{K})|^2. \quad (31)$$

This energy gives a biquadratic coupling that favors perpendicular alignment of upper and lower magnetizations. If the upper surface is rough, there will be an equivalent contribution from the magnetic poles in the upper interface coupling to the lower layer.

For a simple model with one corrugated interface,  $z_L = \delta \cos(2\pi x/L)$ , and one smooth interface  $z_U = D$ , see Fig 10, Eq. (31) gives

$$J_2 \sim -\frac{\mu_0^2 M_s^4 L \delta^2}{A_{\text{ex}}} e^{-4\pi D/L} \quad (32)$$

provided the lower magnetization is perpendicular to the corrugation. This interaction favors very long period roughness. When the ferromagnetic films have finite thicknesses, this contribution to the biquadratic coupling becomes weaker, the opposite behavior from that found for the biquadratic coupling in Eq. (24). In the latter case, the thinner ferromagnetic films allow the fluctuations to increase because the driving force for the fluctuations acts only at the interface. On the other hand, in Eq. (31) the driving force for the fluctuations acts throughout film, so that making the film thinner reduces the net effect of the fluctuations.

Evidence for this mechanism of biquadratic coupling comes from measurements of its thickness dependence [119] in Fe/Ag/Fe samples grown on GaAs. The authors compared the experimental results with a model equivalent to Eq. (31) and found good agreement using roughness parameters consistent with the measured roughness. Additional evidence comes from the observation that for most wedges grown on Fe whiskers, biquadratic coupling dominates in the thickest parts of the wedge [120]. Here, other mechanisms are expected to become weaker as spacer layers become thicker. The magnetostatic coupling is dominated by long wavelength roughness making the exponential damping less effective at limiting the coupling. For thick spacer layers, where other interactions have become small, this form of biquadratic coupling is likely to be the dominant interaction.

A study of an amorphous spacer layer showed evidence for both orange-peel coupling and magnetostatic biquadratic coupling [121]. For thin layers, the magnetizations of the two layers are parallel in the ground state, but as the thickness of the spacer increases, the alignment crosses over to perpendicular. The authors were able to fit the results to a combination of these two coupling measurements using a roughness consistent with that measured by scanning tunneling microscopy.

#### 4.4 Loose spins

Many measurements of biquadratic coupling show a very strong temperature dependence. On the other hand, the bilinear coupling and the magnetization generally vary slowly with temperature, so that inserting their temperature

dependence into the expressions for biquadratic coupling, Eq. (22) and Eq. (31), gives only weak dependence. Slonczewski [122] has developed a “loose spin” mechanism that does show a strong temperature dependence. While the argument that the other types of coupling do not show a strong temperature dependence may be overly simplistic, the loose spin model has been established in samples constructed specifically to test for it.

To produce a strong temperature dependence, Slonczewski postulates the existence of magnetic moments (spins) that are only weakly coupled to the magnetic layers. There is no direct exchange coupling, only the indirect exchange coupling mediated by the spacer layer electrons. These weakly coupled spins are paramagnetic. However, they see a potential that is anisotropic due to their coupling to the magnetic layers

$$V(\hat{\mathbf{m}}) = J_L \widehat{\mathbf{M}}_L \cdot \hat{\mathbf{m}} + J_U \widehat{\mathbf{M}}_U \cdot \hat{\mathbf{m}}, \quad (33)$$

where  $L$  ( $U$ ) refers to the lower (upper) layer. Note that the potential depends on the relative orientation of the magnetizations of the two layers. To see the origin of biquadratic coupling, consider a zero-temperature, classical treatment of the loose spin. At zero temperature, a classical spin will be in its minimum energy configuration. Since the energy of the minimum depends on the relative orientation of the layer magnetizations, the loose spin contributes an effective interaction between magnetizations which can be expanded in powers of the relative orientation

$$J = \sum_{n=1}^{\infty} (-1)^n N_n \frac{(J_L J_U)^n}{(J_L^2 + J_U^2)^{n-1/2}} (\widehat{\mathbf{M}}_L \cdot \widehat{\mathbf{M}}_U)^n. \quad (34)$$

The bilinear term,  $n = 1$  favors either parallel or antiparallel alignment of the magnetizations depending on the relative sign of  $J_L$  and  $J_U$ . The biquadratic piece always favors perpendicular alignment. The numerical factors  $N_n$  are such that the bilinear term always wins. A single loose spin always gives a dominant bilinear coupling. However, for a collection of loose spins, the signs of  $J_L$  and  $J_U$  can vary. In this case, the bilinear contributions may cancel out, leaving a dominant biquadratic coupling.

At finite temperature, the fraction of the time each spin spends close to its minimum energy orientation depends strongly on temperature. Its paramagnetic behavior gives a strong temperature dependence to the coupling, Eq. (34). At temperatures high compared to the potential minimum, the spin will have an isotropic orientation distribution, and the effective coupling mediated by the loose spin will go to zero. Since the loose spin is not directly coupled to the magnetic layer, the temperature scale of the coupling will be much lower than the Curie temperature of the magnetic layers.

The existence of this coupling mechanism has been tested in experiments in which magnetic atoms have been intentionally introduced at low densities into the spacer layer [123, 124, 125]. Agreement with the loose spin model was found in [125]; this experiment used the lowest density of loose spins. The authors speculate that the higher densities used in the other publications obscured the behavior expected from the model.

## 4.5 Torsion model

If the spacer layer is antiferromagnetic, none of the models discussed above are sufficient to describe the coupling. For ideal multilayers, the coupling is simply the result of the direct coupling from layer to layer in the antiferromagnet. However, it is impossible to avoid thickness fluctuations so the coupling will be frustrated. Slonczewski introduced the “torsion model” [11] to describe frustrated antiferromagnetic spacer layers.

The torsion model is based on the following model of the behavior for an ideal system of two ferromagnetic layers separated by an antiferromagnetic spacer. All moments are assumed to remain in plane, and can be described by an azimuthal angle  $\phi_j$ . When the relative directions of the magnetizations in the ferromagnets are rotated away from their minimum energy configuration, a spiral winds up in the antiferromagnet. For an  $n + 1$  layer spacer, taking  $n$  to be even for the present, the minimum energy angles for the ferromagnetic layer are  $\phi_L = \phi_U$ . When the magnetization of the top layer is rotated through an angle  $\Delta\phi$ , the magnetizations in the  $j$ th layer in the antiferromagnet are

$$\phi_j = j \frac{\Delta\phi}{n+2} + \phi_j^{\text{AF}}. \quad (35)$$

The first term gives the spiraling of the magnetization, and the second term,  $\phi_j^{\text{AF}} = 0, \pi$  for  $j$  even or odd, gives the antiferromagnetic reversal from layer to layer. I have assumed that the exchange interaction between the ferromagnetic layer and the antiferromagnetic layer is the same as the exchange between layers in the antiferromagnet.

The exchange energy due to the spiral structure is  $-(n+2)J_{\text{AF}} \cos(\Delta\phi/(n+2))$ . When  $n$  is large enough, a small angle expansion of this energy gives a constant term plus

$$E_{n+1} = \frac{J_{\text{AF}}}{2(n+2)}(\Delta\phi)^2. \quad (36)$$

For an  $n$  layer spacer, the minimum energy configuration has  $\phi_{\text{L}} = \phi_{\text{U}} + \pi$ . If the magnetization of the upper layer is rotated so that it makes an angle  $\Delta\phi$  with respect to magnetization of the lower layer, the energy is

$$E_n = \frac{J_{\text{AF}}}{2(n+1)}(\pi - \Delta\phi)^2. \quad (37)$$

When  $n$  is large enough that this model does not break down, both of these energies vary quadratically in the rotation angle rather than as the cosine of the rotation angle.

If the growth front has areas of thickness  $n$  and  $n+1$ , the coupling will be frustrated. In terms of the fractional area of thickness  $n$ ,  $\theta_n$ , the net coupling energy is

$$J = \theta_{n+1} \frac{J_{\text{AF}}}{2(n+2)}(\Delta\phi)^2 + \theta_n \frac{J_{\text{AF}}}{2(n+1)}(\pi - \Delta\phi)^2 \quad (38)$$

The quadratic dependence leads to different behavior in the presence of thickness fluctuations than was found for the cosine dependence of the usual bilinear coupling. For the case of bilinear coupling, the net bilinear coupling can dominate the biquadratic coupling giving parallel or antiparallel alignment. Such collinear alignment will persist up to some finite amount of interfacial roughness. In the torsion model, any roughness leads to non-collinear coupling, although the degree of non-collinearity can be small.

The torsion model is based on the assumption that nearest-neighbor direct exchange adequately describes the coupling in the antiferromagnet and the coupling of the antiferromagnet to the ferromagnet. It has been shown [126] that it is necessary to include many distant neighbors to describe the spin-wave spectrum of transition metal ferromagnets. It is also clear that such a description is not adequate for an incommensurate antiferromagnet like Cr [110, 127]. On the other hand, this model appears to describe Mn spacer layers well [128, 129, 130, 131, 132, 133, 134] even though a simple nearest-neighbor-exchange model may not be valid.

## 5 Specific systems

In this section I discuss selected systems that illustrate many of the important issues in interlayer exchange coupling. For a more complete comparison between theory and experiment, see [13]. For a comprehensive compilation of experimental and theoretical results, see [15]. Both those reviews emphasize transition metal systems. For reviews of work on rare earths, see [135, 136].

### 5.1 Co/Cu

One of the most extensively studied system is Co/Cu, particularly the (100) orientation. It exhibits many of the difficulties encountered when comparing theory and experiment. In spite of these difficulties, a general consensus of the theoretical behavior has emerged based on total energy calculations as well as asymptotic (and preasymptotic) analyses [67, 69, 73, 74, 81, 82, 137, 138, 139, 140]. As is known from the analysis of the experimental Fermi surface [40], there are two different critical spanning vectors, one associated with the interface zone center that gives a long period oscillation, and one associated with the necks that gives a short period. In the asymptotic regime, the long period oscillation is weak and the short period oscillation is relatively strong. However, for smaller thicknesses, where most experimental measurements are made, preasymptotic corrections become very important and change the asymptotic results quite dramatically.

At the critical point for the long period coupling, the reflection amplitudes for both spins are quite small, hence the weak asymptotic coupling. However for parallel wave vectors *close* to the critical point, the minority-electron reflection becomes close to unity, see Fig. 11. As mentioned above in the discussion following Eq. (13), the parallel wave vectors around the critical point within a region  $\approx \kappa/D$  contribute to the coupling. Thus as  $D$  becomes smaller, the regions with strong reflection contribute to the long period oscillation with preasymptotic corrections, which decay as higher powers of  $D^{-1}$ . For thin spacer layers, the long period coupling strength is found to be

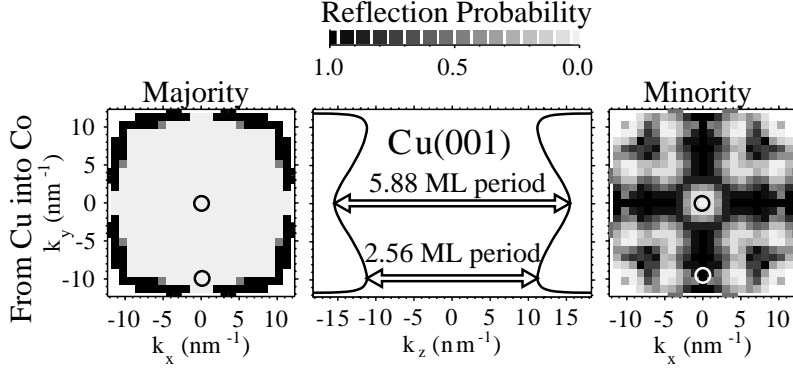


Figure 11: Spin-dependent reflection from Co/Cu(001). The left and right panels show the Fermi surface of Cu shaded based on the reflection probability from Co for majority and minority electrons respectively. The shading scale is given at the top. The Fermi surfaces are projected into the Interface Brillouin zone. The middle panel shows a slice through the Fermi surface and indicates the critical spanning vectors. The projection of the critical spanning vectors are indicated by circles in the left and right panels.

substantial. In addition, since the parts of the Fermi surface making the dominant contribution to the oscillatory coupling have shorter spanning vectors, the apparent period is changed for thin spacer layers as well. Such variation in the periods are generally present, but become more important when the asymptotic coupling is weak and the preasymptotic corrections are significant.

Different asymptotic corrections are important for the short period oscillation in the coupling. At the necks, the reflection probability for the minority electrons is quite strong because there is a symmetry gap for the states in the Co with the symmetry of those on the Cu Fermi surface. However, the gap is fairly narrow in energy. Since the phase of the reflection amplitude changes by  $\pi$  as a function of energy when going from the bottom of a gap to the top, the reflection amplitude (but not the reflection probability) has a strong energy dependence. Evidence for this rapid variation of the phase of the reflection amplitude has been in photoemission studies of Cu on Co [141]. In carrying out the energy integration in Eq. (9), I have neglected the energy dependence of the reflection amplitude. For thin layers, the phase variation of the reflection amplitude makes a substantial correction to the strength of the coupling, typically reducing it.

From these theoretical arguments, analyzing experimental data in terms of the form Eq. (17) cannot be expected to give meaningful results unless the spacer layer thicknesses are in the regime in which the asymptotic approximation is valid. Most measurements [22, 23, 24, 87, 142, 143] are made in the opposite limit. In addition, the roughness of the interfaces can apparently vary significantly from measurement to measurement, hence the sample-to-sample variation found by Weber et al. [87]. The varying roughness and the importance of preasymptotic corrections explains the wide variation in the measured periods for the long period oscillation given in Table 1. Due to the unmeasured effect of interface roughness, it is not surprising that the measured values of the coupling strength are at least a factor of three smaller than the equivalent theoretical results.

## 5.2 Au/Fe and Ag/Fe

As shown in Table 1, the periods measured for Au/Fe and Ag/Fe trilayers [86, 7] grown on Fe whiskers are in remarkable agreement with those predicted from the experimental Fermi surface [40]. To measure the coupling strengths, Unguris et al. [144] used MOKE to measure the coupling strength for Au/Fe on similar samples. The samples were first characterized in zero field by SEMP, including a measurement of the RHEED intensity oscillations to determine the width of the growth front. Using the measured width of the growth front in their analysis, they were able to correct for the averaging of the coupling due to roughness, Eq. (20). Fitting the measured coupling strength to the asymptotic form Eq. (17), they determined the coupling strengths [145],  $J^S/(1 \text{ nm})^2 = 1.29 \text{ mJ/m}^2 \pm 0.16 \text{ mJ/m}^2$  and  $J^L/(1 \text{ nm})^2 = 0.18 \text{ mJ/m}^2 \pm 0.02 \text{ mJ/m}^2$ . The coupling strength has been measured for Ag/Fe [146], but has not been analyzed in terms of the asymptotic form.

There have been far fewer calculations of the coupling for Au/Fe than for Co/Cu [74, 96, 147, 148]. Calculations, which predated the experimental results, of the asymptotic coupling strengths [74] gave  $2.0 \text{ mJ/m}^2$  and  $1.1 \text{ mJ/m}^2$  for

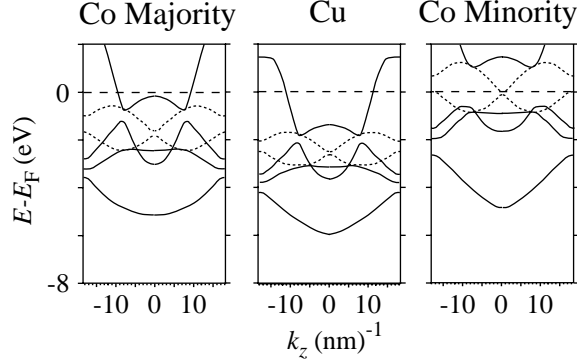


Figure 12: Band structures of Co and Cu. The band structures are shown along the line in the (100) direction through the critical point for the short period coupling. States along this line are either even (solid lines) or odd (dotted lines) with respect to a mirror plane. The two do not couple to each other during reflection and transmission. Thus, electrons at the Fermi energy in Cu see a symmetry gap if they have minority spin, and completely reflect. The phase of the reflection amplitude varies by  $\pi$  from the bottom to the top of the gap. Since the gap is less than 2 eV, the phase variation is substantial.

the short and long periods respectively. The short period coupling strength is within a factor of two the experimental result, but the long period coupling is about a factor of six larger. Recent total energy calculations [96] have cast doubt even on this agreement for the short period coupling. These calculations were analyzed, like the experiment, to extract the effective asymptotic coupling strengths. The extracted values [149], 3.4 mJ/m<sup>2</sup> and 1.1 mJ/m<sup>2</sup> were considerably larger than the experiment for both periods.

There are several possible reasons for the discrepancy in the calculations of the short period coupling strength. At the critical point for the short period, the reflection amplitudes are changing rapidly, which introduces two possible reasons for disagreement. As there has not been an analysis of the preasymptotic corrections for this system, it may be the total energy calculations are not in the asymptotic limit. More likely, the small errors in the Fermi surface as computed in the layer matching calculation [74] may give much larger errors in the coupling due to the rapid variation in the reflection amplitudes. If this explanation is correct, some uncertainty remains in both calculations due to the small errors introduced by the local spin density approximation. Alternatively, the difference may be due to the different treatment of the ferromagnetic layers, semi-infinite for the asymptotic calculation and finite for the total energy calculation. However, total energy calculations [96] in which the ferromagnetic thickness is varied at fixed spacer thickness do not show significant variation.

The common explanation for disagreement between theory and experiment, thickness fluctuations, does not apply to the measurements on this system for two reasons. First, they have been accounted for in the extraction of the coupling strengths from experiment. In addition, thickness fluctuations reduce the short period coupling more than the long period coupling. But to bring the theoretical results into agreement with the measured results, the long period strength needs to be reduced more than that of the short period. Optiz et al. [96] looked at the effect of interfacial defects on the coupling. They found that Au atoms that are interdiffused into the top Fe layer suppress the long period coupling much more strongly than the short period coupling. Such behavior could bring the theoretical results into better agreement with experiment. Au “floating” on top of Fe during growth has been observed [150], making it plausible that there is interdiffusion at the interface.

Other total energy calculations [147, 148] for this system have not been analyzed in terms of the asymptotic form making it difficult to compare them with experiment or other calculations. Since the effective periods extracted from [148] disagree by up to 10 % from the results of [96], it is difficult to compare total energies directly, because the calculations get out of phase with each other. The authors find that the calculated peak positions and relative heights agree well (overall heights disagree by an order of magnitude) with those measured for Au/Fe multilayers grown on GaAs [29]. However, there is substantial disagreement between the results for samples grown on GaAs and those grown on an Fe whisker.

There has been one calculation of the asymptotic coupling for Ag/Fe [74]. Since the experimental results [146] have not been analyzed in terms of the asymptotic form, a detailed comparison is difficult. Roughly, the measured

and calculated couplings are close in magnitude.

### 5.3 Cr/Fe

The other intensively studied system is Cr/Fe, particularly the (100) orientation. Cr/Fe was the first transition metal multilayer system to show interlayer exchange coupling [1], one of the first to show oscillatory interlayer exchange coupling [6], and the first to show short period coupling [25, 26, 27]. Much of the interest in Cr/Fe is due to the close lattice match between Cr and Fe, better than any other transition metal pair (excluding the noble metals discussed above). In addition, Cr/Fe exhibits extremely complicated behavior, much of which arises from the presence of spin-density-wave antiferromagnetism in the Cr. There have been three review articles [110, 151, 152] devoted at least in part to this issue. It is interesting to read all three to compare the interpretation of the same symphony by three different conductors.

In Cr, there are a number of competing phases: paramagnetic, commensurate spin-density wave, incommensurate spin-density wave, and helical spin-density wave. The incommensurate spin-density wave can be longitudinal or transverse. The order propagation vector can be perpendicular to the interface or in the plane of the interface. In bulk Cr, the equilibrium phases are (in order of decreasing temperature): paramagnetic, transverse incommensurate spin-density wave, and longitudinal incommensurate spin-density wave. The equilibrium phase is sensitive to alloying and strain as well as coupling to one or more layers of ferromagnetic Fe. It can be very difficult to distinguish between the different phases experimentally.

Taken at face value, many measurements of Cr/Fe are contradictory. However, it has become clear that the differences arise from the sensitivity of the antiferromagnetic order in Cr to the presence of disorder, particularly at the interfaces. It is possible to construct a consistent picture to explain much of the various behaviors, but it is very difficult to check the picture with detailed theoretical calculations. Approaches, like model free energies [153], that are capable of describing the temperature dependence of the antiferromagnetism in bulk Cr are not flexible enough to realistically describe the behavior near defects. Calculations that can microscopically treat the effect of disorder, like tight-binding approximations [71, 154, 155] or LSDA calculations [156, 157, 158, 159], are either not capable of describing the bulk behavior (tight-binding) or far too computationally expensive to treat relevant system sizes including defects (LSDA).

There are several measurements on this system that make it clear that the model discussed in Section 3 for the interlayer exchange coupling is not adequate to describe the short period coupling in Cr/Fe multilayers. Antiferromagnetism in the Cr has been seen directly by neutron scattering [160, 161]. The temperature and thickness dependence of the coupling [25, 153] has established that the spin-density wave state plays a role in the coupling for at least some systems. While many of the other measurements can be qualitatively understood, the lack of quantitative test of the explanations leaves much of the behavior open to interpretation. I would expect that experiments that test our understanding of Cr/Fe will give many more surprises. However, such experiments can be quite difficult.

Thickness fluctuations obscure the short period oscillations when samples are grown in less than optimal conditions, frequently revealing a long period coupling [25, 26, 162]. The long period coupling is of interest because it is the only well characterized oscillatory coupling in a lattice-matched system with something besides a noble metal as a spacer layer. Cr has a complicated Fermi surface with a large number of critical spanning vectors [66, 88, 89, 163]. There have been a number of proposals for the origin of the long period coupling [101, 157, 164]. Based on asymptotic coupling calculations, analysis of the Fermi surface measured in de Haas-van Alphen measurements, and studies of alloyed spacer layers, a consensus has formed that the ellipsoids centered at the  $N$ -point of the Cr Brillouin zone (see Fig. 13) are responsible for the coupling. The periods extracted from the de Haas-van Alphen measurements in Table 1 are from the  $N$ -centered ellipsoids.

Studies [102, 103] of  $\text{Cr}_{1-x}\text{V}_x$  alloy spacer layers are based on the fact that this alloy modifies the electronic structure (and hence the Fermi surface) without introducing so much bulk scattering that the interlayer exchange coupling is eliminated. Then, the evolution of the period of the oscillatory coupling can be compared with the calculated evolution of the Fermi surface. Both of these studies showed that the period decreased with V concentration and that the only part of the Fermi surface that grew in an appropriate manner was the  $N$ -centered ellipsoid.

Further evidence favoring the  $N$ -centered ellipsoids was found in experiments [165] in which a Au layer was inserted at one of the interfaces in an Fe/Cr multilayer. The long period coupling was dramatically reduced relative to the short period coupling. The Au Fermi surface covers most of the Brillouin zone, overlapping most of the critical spanning vectors of Cr Fermi surface, but it does not overlap the critical points for the  $N$ -centered ellipsoids. The authors attribute the strong suppression of the long period coupling to the exponential decay of the quantum well

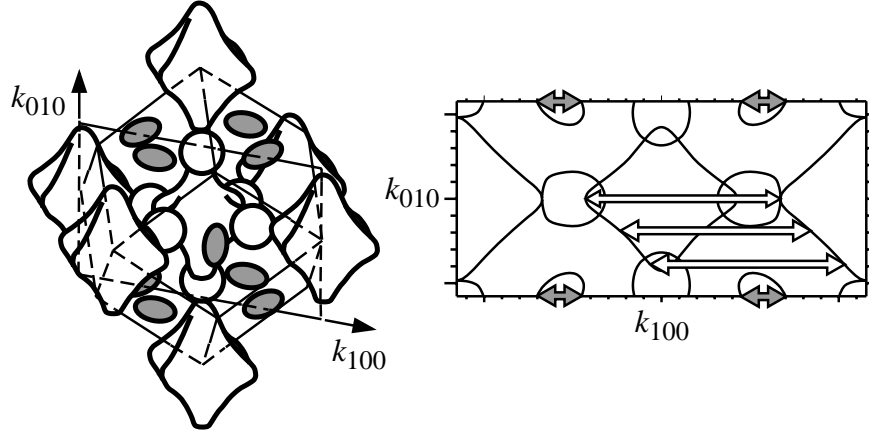


Figure 13: Slice through the Cr Fermi surface. The left panel shows a representation of the Cr Fermi surface in its paramagnetic state. The gray shaded parts are the ellipsoids centered at the N points. Also indicated is a slice through the Fermi surface, which in turn is shown in the right panel. The gray shaded arrows are the critical spanning vectors at the N-centered ellipsoids and the white arrows indicate the nested parts of the Fermi surface that give rise to the spin density wave antiferromagnetism.

states in the gap.

The same oscillation period was observed in (112) oriented systems [90, 166] as in (100) oriented systems and (110) textured systems grown by sputtering [6]. The similarity led to speculation that the oscillation did not originate from Fermi surface properties. However, it turns out that asymptotic coupling calculations, analysis of the Fermi surface measured in de Haas-van Alphen measurements, and studies of alloyed spacer layers all suggest that the N-centered ellipsoids are the origin of the coupling in all three cases.

## 5.4 Fe/Si

While the model presented above has been derived specifically for metallic spacer layers, it has also been extended to insulating or semiconducting spacer layers [67]. The oscillatory coupling is replaced by an exponentially decaying coupling. However, because the preasymptotic corrections may be important, it is conceivable that the sign of the coupling may change once or even twice as a function of spacer layer thickness. The idea of studying coupling through an insulating layer started [167] a large effort in studying coupling through Si and related spacer layers. Here, related refers to the fact the Fe and Si have a strong propensity [168, 169, 170, 171] to form silicides. Much of the effort derives from the fact that many different spacers may develop when these materials combine. Because different silicides can form, it can be very difficult to know what spacer layer is being measured.

There have been a large variety of effects measured. Coupling can be induced by light [172] or heat [173]. In some structures, biquadratic coupling dominates [174, 175], while in some structures with FeSi spacer layers, an oscillatory bilinear coupling has been observed [176]. In a series of nominally pure Si spacer layers a very strong, exponentially decaying coupling decaying coupling has been measured [177], consistent with predictions for insulating spacer layers, which was the original motivation for studying this system. There is apparently still significant disagreement between results in different laboratories and more work needs to be done before these systems are well understood.

## 6 Summary

This review, written from a theorist's point of view, has focused on the physical mechanisms for interlayer coupling in magnetic multilayers. A simple physical picture for interlayer exchange coupling has evolved over the last decade. Spin dependent reflection from the interfaces in multilayers sets up spin-dependent quantum well states. These quantum well states evolve in energy as the thickness of the spacer layer is varied. As these states pass through the Fermi energy, they fill or empty, changing the energy of the multilayer. These changes are periodic because the quantum well states cross the Fermi energy with a period determined by the Fermi surface of the spacer layer

material. At critical points of this Fermi surface, many quantum well states have the same period giving a net oscillatory contribution to the energy. Since the reflection is spin dependent, the energy depends on the relative orientation of the layer magnetizations, i.e., there is an energy difference between parallel and antiparallel alignment of the magnetizations. This energy difference is just the interlayer exchange coupling. It has oscillatory contributions with periods determined by the critical spanning vectors of the spacer layer Fermi surface and strengths determined by the spin-dependent reflection at the interfaces.

This picture for the interlayer exchange coupling has been tested to an extent much greater than the related RKKY coupling between magnetic impurities. For some systems, the periods have been measured to 3 % accuracy. The measured periods agree with those expected from the critical spanning vectors of the Fermi surfaces measured in de Haas-van Alphen experiments. The coupling strengths have been investigated by a number of theoretical techniques and have been measured in carefully prepared samples. There is no completely satisfactory comparison between theory and experiment because there is no system in which a complete characterization of the structure, including all of the defects, has been made. However, enough is understood about the likely defects and their effect on the coupling to give confidence that the physics is correctly described.

While defects confound our ability to compare theory and experiment for the bilinear coupling, they are the origin of biquadratic coupling. Biquadratic coupling, which derives from several mechanisms, appears to be present to some degree in all magnetic multilayers. Two mechanisms arise from interfacial roughness. In one case interfacial roughness gives rise to fluctuations in the strength of the bilinear coupling. In the other it gives rise to an oscillating magnetic field outside the interface. In both cases, the system can lower its energy by allowing the magnetization of the layers to fluctuate in response to the roughness induced variations. The system can lower its energy the most when the two magnetizations are perpendicular to each other, giving an effective coupling that favors perpendicular alignment of the magnetizations.

The study of interlayer exchange coupling has flourished for the past decade and a half. We have developed a clear physical description of the coupling and have successfully compared its predictions with high quality measurements. While very successful, the comparison between theory and experiment is not complete and interesting issues still remain. Successfully addressing these issues requires measuring the coupling in systems that are as close to perfect as possible and then quantitatively measuring all the defects that remain. On the theoretical side, it requires explicitly treating the measured defects. Both aspects of understanding defects are quite difficult and require substantial effort.

## References

- [1] P. Grünberg, R. Schreiber, Y. Pang, M. B. Brodsky, and H. Sowers, *Phys. Rev. Lett.* **57**, 2442 (1986).
- [2] C. F. Majkrzak, J. W. Cable, J. Kwo, M. Hong, D. B. McWhan, Y. Yafet, J. V. Waszczak, and C. Vettier, *Phys. Rev. Lett.* **56**, 2700 (1986).
- [3] M. B. Salamon, S. Sinha, J.J. Rhyne, J. E. Cunningham, R. W. Erwin, J. Borchers, and C. P. Flynn, *Phys. Rev. Lett.* **56**, 259 (1986).
- [4] M. N. Baibich, J. M. Broto, A. Fert, F. Nguyen Van Dau, F. Petroff, P. Etienne, G. Creuzet, A. Friederich, and J. Chazelas, *Phys. Rev. Lett.* **61**, 2472 (1988);
- [5] G. Binasch, P. Grünberg, F. Saurenbach, and W. Zinn, *Phys. Rev. B* **39**, 4828 (1989).
- [6] S. S. P. Parkin, N. More, and K. P. Roche, *Phys. Rev. Lett.* **64**, 2304 (1990).
- [7] J. Unguris, R. J. Celotta, and D. T. Pierce, *J. Appl. Phys.* **75**, 6437 (1994).
- [8] Chapter 2, in *Ultrathin Magnetic Structures II*, edited by B. Heinrich and J. A. C. Bland (Springer-Verlag, Berlin, 1994) p. 45.
- [9] Y. Yafet, in *Magnetic Multilayers*, ed. L. H. Bennett and R. E. Watson (World Scientific, Singapore 1994), p. 19.
- [10] A. Fert, P. Grünberg, A. Barthelemy, F. Petroff, and W. Zinn, *J. Magn. Magn. Mater.* **140-144**, 1 (1995).
- [11] J. C. Slonczewski, *J. Magn. Magn. Mater.* **150**, 13 (1995).
- [12] B. A. Jones, *IBM J. Res. Dev.* **42**, 25 (1998).
- [13] M. D. Stiles, *J. Magn. Magn. Mater.* **200**, 322 (1999).

- [14] P. Bruno, *J. Phys.-Condes. Matter* **11**, 9403 (1999).
- [15] D. E. Bürgler, P. Grünberg, S. O. Demokritov, and M. T. Johnson, in *Handbook of Magnetic Materials, Vol. 13*, ed. K. H. J. Buschow (2001).
- [16] S. S. P. Parkin, *Phys. Rev. Lett.* **67**, 3598 (1991).
- [17] F. Petroff, A. Barthelemy, D. H. Mosca, D. K. Lottis, A. Fert, P. A. Schroeder, W. P. Pratt, R. Loloee, and S. Lequien, *Phys. Rev. B* **44**, 5355 (1991).
- [18] J. Fassbender, F. Nörteman, R. L. Stamps, R. E. Camley, B. Hillebrands, and G. Güntherodt, *Phys. Rev. B* **46**, 5810 (1992).
- [19] K. Ounadjela, D. Miller, A. Dinia, A. Arbaoui, P. Panissod, and G. Suran, *Phys. Rev. B* **45**, 7768 (1992).
- [20] Y. Huai and R. W. Cochrane, *J. Appl. Phys.* **72**, 2523 (1992).
- [21] P. J. H. Bloeman, W. J. M. de Jonge, and R. Coehoorn, *J. Magn. Magn. Mater.* **121**, 306 (1993).
- [22] Z. Q. Qiu, J. Pearson, and S. D. Bader, *Phys. Rev. B* **46**, 8659 (1992);
- [23] M. T. Johnson, S. T. Purcell, N. W. E. McGee, R. Coehoorn, J. aan de Stegge, and W. Hoving, *Phys. Rev. Lett.* **68**, 2688 (1992).
- [24] P. J. H. Bloemen, R. van Dalen, W. J. M. de Jonge, M. T. Johnson, and J. aan de Stegge, *J. Appl. Phys.* **73**, 5972 (1993).
- [25] J. Unguris, R. J. Celotta, and D. T. Pierce, *Phys. Rev. Lett.* **67**, 140 (1991).
- [26] S. Demokritov, J. A. Wolf, and P. Grünberg, *Europhysics Letters* **15**, 881 (1991).
- [27] S. T. Purcell, W. Folkerts, M. T. Johnson, N. W. E. McGee, K. Jager, J. aan de Stegge, W. B. Zeper, and W. Hoving, *Phys. Rev. Lett.* **67**, 903 (1991).
- [28] Z. Celinski and B. Heinrich, *J. Magn. Magn. Mater.* **99**, L25 (1991).
- [29] A. Fuß, S. Demokritov, P. Grünberg, and W. Zinn, *J. Magn. Magn. Mater.* **103**, L221 (1992).
- [30] Y. Wang, P. M. Levy, and J. L. Fry, *Phys. Rev. Lett.* **65**, 2732 (1990).
- [31] M. Rührig, R. Schäfer, A. Hubert, R. Mosler, J. A. Wolf, S. Demokritov, and P. Grünberg, *Phys. Status Solidi A* **125**, 635 (1991).
- [32] B. Heinrich, J. F. Cochran, M. Kowalewski, J. Kirschner, Z. Celinski, A. S. Arrott, and K. Myrtle, *Phys. Rev. B* **44**, 9348 (1991).
- [33] J. C. Slonczewski, *Phys. Rev. Lett.* **67**, 3172 (1991).
- [34] F. J. Himpsel, *Phys. Rev. B* **44**, 5966 (1991). J. E. Ortega and F. J. Himpsel, *Phys. Rev. Lett.* **69**, 844 (1992). J. E. Ortega, F. J. Himpsel, G. J. Mankey, and R. F. Willis, *Phys. Rev. B* **47**, 1540 (1993).
- [35] N. B. Brookes, Y. Chang, and P. D. Johnson, *Phys. Rev. Lett.* **67**, 354 (1991).
- [36] R. K. Kawakami, E. Rotenberg, E. J. Escorcia-Aparicio, H. J. Choi, J. H. Wolfe, N. V. Smith, and Z. Q. Qiu, *Phys. Rev. Lett.* **82**, 4098 (1999).
- [37] Z Q Qiu and N V Smith *J. Phys. Condens. Matter* **14**, R169 (2002).
- [38] In these models, the Fermi surface that determines the properties of the interlayer coupling is the (possibly) fictitious Fermi surface of the material that makes up the non-magnetic spacer layer. A Fermi surface is only truly defined for an infinite periodic solid. However, due to the rapid screening by metals, the potential seen by electrons in the middle of all but the thinnest spacer layers is practically indistinguishable from the potential seen in the interior of an infinite sample of the same material. Since the Fermi surface of an infinite material describes the response to perturbations of the electron system in that potential, that same Fermi surface describes the response to perturbations of the electron system inside the spacer layer. Thus, the oscillatory coupling is determined by the Fermi surface of the material that makes up the spacer layer, which is well defined, and not the Fermi surface of the spacer layer itself.
- [39] M. A. Ruderman and C. Kittel, *Phys. Rev.* **96**, 99 (1954); T. Kasuya, *Prog. Theor. Phys.* **16**, 45, 58 (1956); K. Yosida, *Phys. Rev.* **106**, 893 (1957).

- [40] P. Bruno and C. Chappert, Phys. Rev. Lett. **67**, 1602 (1991).
- [41] R. Coehoorn, Phys. Rev. B **44**, 9331 (1991).
- [42] D. M. Deaven, D. S. Rokhsar, and M. Johnson, Phys. Rev. B **44**, 5977 (1991).
- [43] C. Chappert and J. P. Renard, Europhys. Lett. **15**, 553 (1991).
- [44] Y. Yafet, J. Appl. Phys. **61**, 4058 (1987); Y. Yafet, J. Kwo, M. Hong, C. F. Majkrzak, and T. O'Brien, J. Appl. Phys. **63**, 3453 (1988).
- [45] Z.-P. Shi, P. M. Levy, and J. L. Fry, Phys. Rev. Lett. **69**, 3678 (1992).
- [46] C. Lacroix and J. P. Gavigan, J. Mag. Mag. Mater. **93**, 413 (1991).
- [47] P. Bruno, J. Mag. Mag. Mater. **116**, L13 (1992).
- [48] J. R. Cullen and K. B. Hathaway, J. Appl. Phys. **70**, 5879 (1991). K. B. Hathaway and J. R. Cullen, J. Magn. Mater. **104-107**, 1840 (1992).
- [49] J. Barnaś, J. Magn. Magn. Mater. **111**, L215 (1992).
- [50] D. M. Edwards, J. Mathon, R. B. Muniz, and M. S. Phan, Phys. Rev. Lett. **67**, 493 (1991).
- [51] R. F. C. Farrow, IBM J. Res. Dev. **42**, 43 (1998).
- [52] Q. Leng, V. Cros, R. Schäfer, A. Fuß, P. Grünberg, and W. Zinn, J. Magn. Magn. Mater. **126**, 367 (1993);
- [53] Z. Celinski, B. Heinrich, J. F. Cochran, W. B. Muir, A. S. Arrott, and J. Kischner, Phys. Rev. Lett. **65**, 1156 (1990); E. Fullerton, D. Stoeffler, K. Ounadjela, B. Heinrich, and Z. Celinski, Phys. Rev. B **51**, 6364 (1995).
- [54] J. E. Mattson, C. H. Sowers, A. Berger, and S. D. Bader, Phys. Rev. Lett. **68**, 3252 (1992).
- [55] M. E. Brubaker, J. E. Mattson, C. H. Sowers, and S. D. Bader, App. Phys. Lett. **58**, 2306 (1991).
- [56] A. Davies, J. A. Stroschio, D. T. Pierce, and R. J. Celotta, Phys. Rev. Lett. **76**, 4175 (1996).
- [57] D. Venus and B. Heinrich, Phys. Rev. B **53**, R1733 (1996).
- [58] R. Pfandzelter, T. Igel, and H. Winter, Phys. Rev. B **54**, 4496 (1996).
- [59] V. M. Uzdin, W. Keune, H. Schror, M. Walterfang, Phys. Rev. B **63**, 4407 (2001).
- [60] D. D. Chambliss, R. J. Wilson, and S. Chiang, IBM J. Res. Dev. **39**, 639 (1995).
- [61] J. A. Stroschio and D. T. Pierce, J. Vac. Sci. Technol. B **12**, 1783 (1994).
- [62] D. E. Bürgler, C. M. Schmidt, D. M. Schaller, F. Meisinger, R. Hofer, and H.-J. Güntherodt, Phys. Rev. B **56**, 4149 (1997).
- [63] T. L. Monchesky, B. Heinrich, R. Urban, K. Myrtle, M. Klaua, and J. Kirschner, Phys. Rev. B **60**, 10242 (1999).
- [64] B. Heinrich and J. F. Cochran, Adv. Phys. **42**, 523 (1993).
- [65] P. Bruno, J. Magn. Magn. Mater. **121**, 238 (1993).
- [66] M. D. Stiles, Phys. Rev. B **48**, 7238 (1993).
- [67] P. Bruno, Phys. Rev. B **52**, 411 (1995).
- [68] J. Mathon, M. Villeret, and D. M. Edwards, J. Phys. Condens. Matter **4** 9873, (1992).
- [69] F. Herman, J. Sticht, and M. Van Schilfgaarde, J. Appl. Phys. **69**, 4783 (1991).
- [70] K. Ounadjela, C. B. Sommers, A. Fert, D. Stoeffler, F. Gautier, and V. L. Moruzzi, Europhysics Letters **15**, 875 (1991).
- [71] D. Stoeffler and F. Gautier, Progress of Theoretical Physics Supplement **101**, 139 (1990); D. Stoeffler and F. Gautier, Phys. Rev. B **44**, 10389 (1991).
- [72] H. Hasegawa, Phys. Rev. B **42**, 2368 (1990); H. Hasegawa, Phys. Rev. B **43**, 10803 (1991).

- [73] B. Lee and Y.-C. Chang, Phys. Rev. B **51**, 316 (1995); B. C. Lee, Y. C. Chang, Phys. Rev. B **62**, 3888 (2000).
- [74] M. D. Stiles, J. Appl. Phys. **79**, 5805 (1996).
- [75] K. M. Schep, J. B. A. N. van Hoof, P. J. Kelly, G. E. W. Bauer, and J. E. Inglesfield, Phys. Rev. B **56**, 10805 (1997).
- [76] I. Riedel, P. Zahn, and I. Mertig, Phys. Rev. B **63**, 195403 (2001).
- [77] P. D. Johnson, Rep. Prog. Phys. **60**, 1217 (1997).
- [78] F. J. Himpsel, T. A. Jung, and P. F. Seidler, IBM J. Res. Dev. **42**, 33 (1998).
- [79] K. Garrison, Y. Chang, and P. D. Johnson, Phys. Rev. Lett. **71**, 2801 (1993).
- [80] M. S. Ferreira, J. d'Albuquerque e Castro, D. M. Edwards and J. Mathon, J. Phys. Condens. Matter **8** 11259, (1996).
- [81] J. Mathon, M. Villeret, R. B. Muniz, J. d'Albuquerque e Castro, and D. M. Edwards, Phys. Rev. Lett. **74**, 3696 (1995); J. Mathon, M. Villeret, A. Umerski, R. B. Muniz, J. d'Albuquerque e Castro, and D. M. Edwards, Phys. Rev. B **56**, 11797 (1997).
- [82] P. Bruno, Eur. Phys. J. B **11**, 83 (1999).
- [83] P. J. H. Bloemen, M. T. Johnson, M. T. H. van de Vorst, R. Coehoorn, J. J. de Vries, R. Jungblut, J. aan de Stegge, A. Reinders, and W. J. M. de Jonge, Phys. Rev. Lett. **72**, 764 (1994).
- [84] S. N. Okuno and K. Inomata, Phys. Rev. B **51**, 6139 (1995).
- [85] J. J. de Vries, A. A. P. Schudelar, R. Jungblut, P. J. H. Bloemen, A. Reinders, J. Kohlhepp, R. Coehoorn, and W. J. M. de Jonge, Phys. Rev. Lett. **75**, 4306 (1995).
- [86] J. Unguris, R. J. Celotta, and D. T. Pierce, J. Magn. Magn. Mater. **127**, 205 (1993).
- [87] W. Weber, R. Allenpach, and A. Bischof, Europhys. Lett. **31**, 491 (1995).
- [88] M. D. Stiles, Phys. Rev. B **54**, 14679 (1996).
- [89] L. Tsetseris, B. Lee, and Y.-C. Chang, Phys. Rev. B **55**, 11586 (1997); L. Tsetseris, B. Lee, and Y.-C. Chang, Phys. Rev. B **56**, R11392 (1997).
- [90] E. E. Fullerton, M. J. Conover, J. E. Mattson, C. H. Sowers, and S. D. Bader, Phys. Rev. B **48**, 15755 (1993).
- [91] A. H. MacDonald, T. Jungwirth, and M. Kasner, Phys. Rev. Lett. **81**, 705 (1998).
- [92] J. Inoue, Phys. Rev. B **50**, 13541 (1994).
- [93] J. Kudrnovský, V. Drchal, I. Turek, M. Šob, and P. Weinberger, Phys. Rev. B **53**, 5125 (1996).
- [94] M. Freyss, D. Stoeffler, and H. Dreyssé, Phys. Rev. B **54**, 12667 (1996).
- [95] A. T. Costa, J. D. E. Castro, R. B. Muniz, Phys. Rev. B **59**, 11424 (1999).
- [96] J. Opitz, P. Zahn, J. Binder, I. Mertig, Phys. Rev. B **6309**, 4418 (2001).
- [97] P. Zahn, I. Mertig, Phys. Rev. B **6310**, 4412 (2001).
- [98] R. K. Nesbet, J. Phys. Cond. Mat. **6**, L449 (1994). R. K. Nesbet, Int. J. Quantum Chem. Symp. **28**, 77 (1995).
- [99] S. S. P. Parkin, C. Chappert, and F. Herman, Europhys. Lett. **24**, 71 (1993).
- [100] S. N. Okuno and K. Inomata, Phys. Rev. Lett. **70**, 1711 (1993).
- [101] M. van Schilfgaarde, F. Herman, S. S. P. Parkin, and J. Kudrnovský, Phys. Rev. Lett. **74**, 4063 (1995).
- [102] C.-Y. You, C. H. Sowers, A. Inomata, J. S. Jiang, S. D. Bader, and D. D. Koelling, J. Appl. Phys. (to be published).
- [103] N. N. Lathiotakis, B. L. Gyorffy, E. Bruno, B. Ginatempo, and S. S. P. Parkin, Phys. Rev. Lett. **83**, 215 (1999).
- [104] J. Kudrnovský, V. Drchal, P. Bruno, I. Turek, and P. Weinberger, Phys. Rev. B **54**, R3738 (1996).

- [105] N. N. Lathiotakis, G. L. Györffy, J. B. Staunton, and B. Újfalussy, *J. Magn. Magn. Mater.* **185**, 293 (1998).
- [106] R. P. Erickson, K. B. Hathaway, and J. R. Cullen, *Phys. Rev. B* **47**, 2626 (1993).
- [107] J. Barna and P. Grünberg, *J. Magn. Magn. Mater.*, **121**, 326 (1993).
- [108] D. M. Edwards, J. M. Ward, and J. Mathon, *J. Magn. Magn. Mater.*, **126**, 380 (1993).
- [109] M. D. Stiles, Unpublished.
- [110] D. T. Pierce, J. Unguris, R. J. Celotta, M. D. Stiles, *J. Magn. Magn. Mater.* **200**, 290 (1999).
- [111] J. F. Bobo, H. Kikuchi, O. Redon, E. Snoeck, M. Piecuch, R. L. White, *Phys. Rev. B* **60**, 4131 (1999).
- [112] L. Néel, *C. R. Hebd. Seances Acad. Sci.* 255, 1545 (1962); L. Néel, *C. R. Hebd. Seances Acad. Sci.* 255, 1676 (1962).
- [113] J. C. S. Kools, W. Kula, D. Mauri, T. Lin, *J. Appl. Phys.* **85**, 4466 (1999).
- [114] H. D. Chopra, D. X. Yang, P. J. Chen, D. C. Parks, W. F. Egelhoff, *Phys. Rev. B* **61**, 9642 (2000).
- [115] B. D. Schrag, A. Anguelouch, S. Ingvarsson, G. Xiao, Y. Lu, P. L. Trouilloud, A. Gupta, R. A. Wanner, W. J. Gallagher, P. M. Rice, and S. S. P. Parkin, *Appl. Phys. Lett.* **77**, 2373 (2000).
- [116] S. Tegen, I. Monch, J. Schumann, H. Vinzelberg, C. M. Schneider, *J. Appl. Phys.* **89**, 8169 (2001).
- [117] J. Langer, R. Mattheis, B. Ocker, W. Maass, S. Senz, D. Hesse, and J. Krausslich, *J. Appl. Phys.* **90**, 5126 (2001).
- [118] S. Demokritov, E. Tsymbal, P. Grünberg, W. Zinn, and I. K. Schuller, *Phys. Rev B* **49**, 720 (1994).
- [119] U. Rücker, S. O. Demokritov, E. Tsymbal, P. Grünberg, and W. Zinn, *J. Appl. Phys.* **78**, 387 (1995).
- [120] J. Unguris, Private Communication.
- [121] P. Fuchs, U. Ramsperger, A. Vaterlaus, M. Landolt, *Phys. Rev. B* **55** 12546 (1997).
- [122] J. C. Slonczewski *J. Appl. Phys.* **73**, 5957 (1993).
- [123] B. Heinrich, Z. Celinski, L. X. Liao, M. From and J. F. Cochran, *J. Appl. Phys.* **75**, 6187 (1994).
- [124] J. J. de Vries, G. J. Strikers, M. T. Johnson, A. Reinders, and W. J. M. de Jonge, *J. Magn. Magn. Mater.* **148**, 187 (1995).
- [125] M. Schäfer, S. O. Demokritov, S. O. Müller-Pfeiffer, R. Schäfer, M. Schneider, P. Grünberg, and W. Zinn, *J. Appl. Phys.* **77**, 6432 (1995). Sc95
- [126] S. V. Halilov, H. Eschrig, A. Y. Perlov, and P. M. Oppeneer *Phys. Rev. B* **58**, 293 (1998).
- [127] B. Heinrich, J. F. Cochran, T. Monchesky, R. Urban, *Phys. Rev. B* **59**, 14520 (1999).
- [128] S. T. Purcell, M. T. Johnson, N. W. E. McGee, R. Coehoorn, and W. Hoving, *Phys. Rev. B* **45**, 13064 (1992).
- [129] M. E. Filipkowski, J. J. Krebs, G. A. Prinz, C. J. Gutierrez, *Phys. Rev. Lett.* **75**, 1847 (1995).
- [130] T. Monchesky, B. Heinrich, J. F. Cochran, and M. Klaua, *J. Magn. Magn. Mat.* **198-199**, 421 (1999).
- [131] S. Yan, R. Schreiber, F. Voges, C. Osthöver, and P. Grünberg, *Phys. Rev. B* **59**, R11641 (1999).
- [132] D. A. Tulchinsky, J. Unguris, and R. J. Celotta, *J. Magn. Magn. Mater.* **212**, 91-100 (2000).
- [133] D.T. Pierce, A. D. Davies, J. A. Stroschio, D. A. Tulchinsky, J. Unguris, and R. J. Celotta, *J. Magn. Magn. Mater.* **222**, 13 (2000).
- [134] S. S. Yan, P. Grünberg, R. Schäfer, *Phys. Rev. B* **62**, 5765 (2000).
- [135] C. F. Majkrzak, J. Kwo, M. Hong, Y. Yafet, D. Gibbs, C. L. Chein, and J. Bohr, *Adv. Phys.* **40**, 99 (1991).
- [136] J. J. Rhyne and R. W. Erwin, in *Magnetic Materials*, Vol. 8, ed. K. H. J. Buschow (North-Holland, Elsevier, Amsterdam, 1995) p. 1.

- [137] P. Lang, L. Nordström, R. Zeller, and P. H. Dederichs, Phys. Rev. Lett. **71**, 1927 (1993); L. Nordström, P. Lang, R. Zeller, and P. H. Dederichs, Phys. Rev. B **50**, 13058 (1994); P. Lang, L. Nordström, K. Wildberger, R. Zeller, P.H. Dederichs, and T. Hoshino, Phys. Rev. B **53**, 9092 (1996);
- [138] J. Kudrnovský, V. Drchal, I. Turek, and P. Weinberger, Phys. Rev. B **50**, 16105 (1994); V. Drchal, J. Kudrnovský, I. Turek, and P. Weinberger, Phys. Rev. B **53**, 15036 (1996). V. Drchal, J. Kudrnovsky, P. Bruno, I. Turek, P. H. Dederichs, and P. Weinberger, Phys. Rev. B **60**, 9588 (1999).
- [139] K. Wildberger, R. Zeller, P. H. Dederichs, J. Kudrnovský, and P. Weinberger, Phys. Rev. B **58**, 13721 (1998).
- [140] N. N. Lathiotakis, B. L. Gyorffy, B. Ujfalussy, Phys. Rev. B **61**, 6854 (2000).
- [141] A. Danese, D. A. Arena, R. A. Bartynski, Prog. Surf. Sci. **67**, 249 (2001).
- [142] A. Cebollada, R. Miranda, C. M. Schneider, P. Schuster, and J. Kirschner, J. Magn. Magn. Mater. **102**, 25 (1991).
- [143] C. Stamm, Ch. Wüsch, S. Egger, and D. Pescia, J. Magn. Magn. Mater. **177-181**, 1279 (1998).
- [144] J. Unguris, R.J. Celotta, and D.T. Pierce, Phys. Rev. Lett. **79**, 2734 (1997).
- [145] The asymptotic coupling strengths are reported in mJ/m<sup>2</sup> by evaluating  $J^\alpha/D^2$  at an effective thickness of  $D = 1$  nm.
- [146] Z. Celinski, B. Heinrich, and J. F. Cochran, J. Appl. Phys. **73**, 5966 (1993).
- [147] L. Szunyogh, B. Ujfalussy, P. Weinberger, C. Sommers, Phys. Rev. B **54**, 6430 (1996)
- [148] A. T. Costa, J. d'Albuquerque e Castro, and R. B. Muniz, Phys. Rev. B **56**, 13697 (1997).
- [149] The values quoted here differ from the values given in [96] because of a different convention used for the definition of  $J$ .
- [150] E. R. Moog, C. Liu, S. D. Bader, and J. Zak, Phys. Rev. B **39**, 6949 (1989)
- [151] H. Zabel, J. Phys.-Condens. Matter. **11**, 9303 (1999)
- [152] R. S. Fishman, J. Phys.-Condens. Matter **13**, R235 (2001).
- [153] Z.-P. Shi and R. S. Fishman, Phys. Rev. Lett. **78**, 1351 (1997); R. S. Fishman and Z.-P. Shi, Phys. Rev. B **59**, 1384 (1999).
- [154] M. Freyss, D. Stoeffler, H. Dreyse, Phys. Rev. B **54**, 12677 (1996); M. Freyss, D. Stoeffler, H. Dreyse, Phys. Rev. B **56**, 6047 (1997); C. Cornea, D. Stoeffler, Europhys. Lett. **49**, 217 (2000); D. Stoeffler, C. Cornea, Europhys. Lett. **56**, 282 (2001).
- [155] A. T. Costa, A. C. D. Barbosa, J. D. E. Castro, R. B. Muniz, J. Phys.-Condens. Matter **13**, 1827 (2001).
- [156] M. van Schilfgaarde and F. Herman, Phys. Rev. Lett. **71**, 1923 (1993).
- [157] S. Mirbt, A. M. N. Niklasson, H. L. Skriver, and B. Johansson, Phys. Rev. B **54**, 6382 (1996).
- [158] A. M. N. Niklasson, B. Johansson, L. Nordstrom, Phys. Rev. Lett. **82**, 4544 (1999).
- [159] K. Hirai, J. Phys. Soc. Jpn. **70**, 841 (2001).
- [160] A. Schreyer, J. F. Ankner, Th. Zeidler, H. Zabel, C. F. Majkrzak, M. Schäfer, and P. Grünberg Europhys. Lett. **32**, 595 (1995); A. Schreyer, J. F. Ankner, Th. Zeidler, H. Zabel, M. Schäfer, J. A. Wolf, P. Grünberg, and C.F. Majkrzak, Phys. Rev. B **52**, 16066 (1995); A. Schreyer, C. F. Majkrzak, Th. Zeidler, T. Schmitte, P. Bödeker, K. Theis-Bröhl, A. Abromeit, J. A. Dura, and T. Watanabe Phys. Rev. Lett. **79**, 4914 (1997).
- [161] S. Adenwalla, G. P. Felcher, E. E. Fullerton, and S. D. Bader Phys. Rev. B **53**, 2474 (1996); E. E. Fullerton, S. Adenwalla, G. P. Felcher, K. T. Riggs, C. H. Sowers, S. D. Bader, and J. L. Robertson, Physica B **221**, 370 (1996); E. E. Fullerton, S. D. Bader, and J. L. Robertson, Phys. Rev. Lett. **77**, 1382 (1996).
- [162] D. T. Pierce, J. A. Stroschio, J. Unguris, and R. J. Celotta, Phys. Rev. B **49**, 14564 (1994).
- [163] D. D. Koelling, Phys. Rev. B **50**, 273 (1994); D. D. Koelling, Phys. Rev. B **59**, 6351 (1999).
- [164] M. van Schilfgaarde and W. A. Harrison, Phys. Rev. Lett. **71**, 3870 (1993).

- [165] D. E. Bürgler, F. Meisinger, C. M. Schmidt, D. M. Schaller, H. J. Guntherodt, and P. Grünberg, *Phys. Rev. B* **60**, R3732 (1999).
- [166] X. Bian, H. T. Hardner, and S. S. P. Parkin, *J. Appl. Phys.* **79**, 4980 (1996).
- [167] S. Toscano, B. Briner, H. Hopster, and M. Landolt, *J. Magn. Magn. Mater.* **114**, L6 (1992).
- [168] E. E. Fullerton, J. E. Mattson, S. R. Lee, C. H. Sowers, Y. Y. Huang, G. Felcher, S. D. Bader, and F. T. Parker, *J. Magn. Magn. Mater.* **117**, L301 (1992).
- [169] A. Chaiken, R. P. Michel, and M. A. Wall, *Phys. Rev. B* **53**, 5518 (1996).
- [170] R. Kläsches, C. Carbone, and W. Eberhardt, C. Pampuch, O. Rader, T. Kachel, and W. Gudat, *Phys. Rev. B* **56**, 10801 (1997).
- [171] Y. Endo, O. Kitakami, and Y. Shimada, *Phys. Rev. B* **59**, 4279 (1999).
- [172] B. Briner and M. Landolt, *Z. Phys. B* **92**, 137 (1993).
- [173] B. Briner and M. Landolt, *Europhys. Lett.* **28**, 65 (1994); M. Hunziker and M. Landolt, *Phys. Rev. B* **64**, 134421 (2001).
- [174] Y. Saito, K. Inomata, *J. Phys. Soc. Jpn.* **67**, 1138 (1998).
- [175] G. J. Strijkers, J. T. Kohlhepp, H. J. M. Swagten, W. J. M. de Jonge, *Phys. Rev. Lett.* **84**, 1812 (2000).
- [176] R. R. Gareev, D. E. Bürgler, M. Buchmeier, D. Olligs, R. Schreiber, and P. Grünberg, *Phys. Rev. Lett.* **87**, 7202 (2001).
- [177] R. R. Gareev, D. E. Bürgler, M. Buchmeier, R. Schreiber, and P. Grünberg, *J. Magn. Magn. Mater.* (to be published).